CHALMERS
UNIVERSITY OF TECHNOLOGY

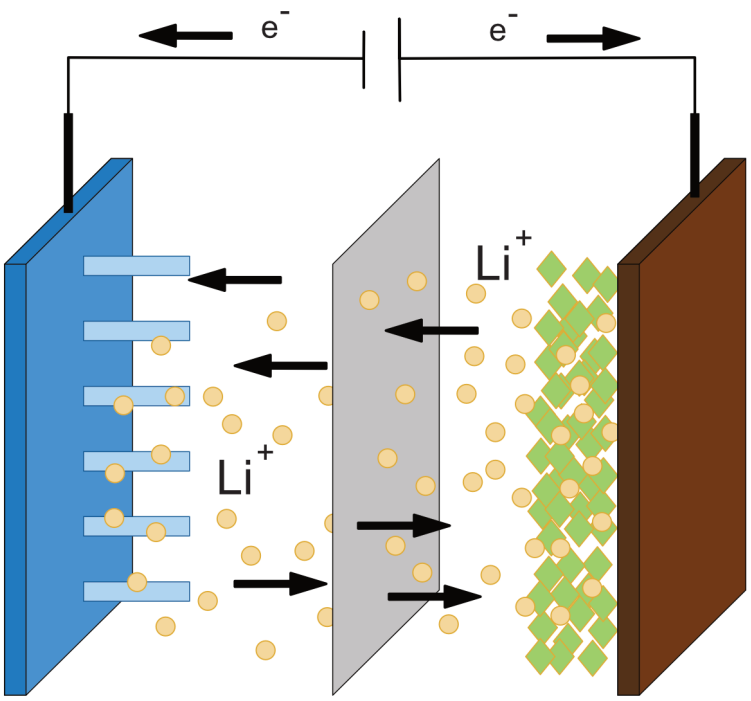

Hybrid Modeling of High-Voltage Battery Systems for Software Control

Master´s thesis report in Sustainable power engineering and electromobility

Felix Gråhn
Jakob Hogander

DEPARTMENT OF ELECTRICAL ENGINEERING
CHALMERS UNIVERSITY OF TECHNOLOGY
Gothenburg, Sweden 2025
www.chalmers.se

Master's Thesis 2025

Hybrid Modeling of High-Voltage Battery Systems for Software Control

Felix Gråhn & Jakob Hogander

CHALMERS
UNIVERSITY OF TECHNOLOGY

Department of Electrical Engineering
Electric Power Engineering
Chalmers University of Technology
Gothenburg, Sweden 2025

Hybrid Modeling of High-Voltage Battery Systems for Software Control

Felix Gråhn & Jakob Hogander

Supervisor: Leonardo Amato, Volvo Cars Corporation
Examiner: Torbjörn Thiringer, Department of Electrical Engineering

Master´s thesis 2025
Department of Electrical Engineering
Chalmers University of Technology
SE-412 96 Gothenburg
Sweden
Telephone +46 31 772 1000

Gothenburg, Sweden 2025

Hybrid Modeling of High-Voltage Battery Systems for Software Control

Felix Gråhn
Jakob Hogander

Department of Electrical Engineering
Chalmers University of Technology

Abstract

In recent years, electric vehicles have taken up a greater part of the automotive industry. This thesis investigated the potential of using a hybrid approach to modeling the behavior of batteries used in electric vehicles on pack level. Using existing models, both empirical and physics-based, to create a model meant for software control. The aim was to find a way to model the aging of batteries and control the battery pack based on internal electrochemical dynamics but at a lower computational load than that of fully physics-based modeling.

During the project, it was shown that the use of a hybrid model to simulate batteries on pack level is a working method that possesses the ability to control on the basis of physics-based dynamics of the batteries. Using a physics-based controller for fast charging of the battery pack was also shown to decrease fast charging time 18 % compared to using a fast charging protocol based on testing. This was possible without compromising the risks of aging. It was also shown that one can not only use the model to evaluate the performance of aged batteries, but also be able to see the aging effects that a given use of the battery has. The hybrid model was also found to operate on a substantially lower computational load. compared to a fully physical-based model, making it possible to run longer simulations.

Keywords: Physics-based modeling, Lithium-ion batteries, SPMe, ECM, Aging, Lithium plating, Current control, Fast charge, Cycling.

Acknowledgements

This work was carried out at the Department of Electrical Engineering at Chalmers University of Technology in collaboration with Volvo Cars Company. Firstly we would like to thank the system and architect team at Volvo Cars Company for letting us do our thesis with them. A special thanks goes out to our supervisor Leonardo Amato for all the feedback and enthusiasm in our project. We would like to thank the technical expert at Volvo cars, Björn Fridholm, for his advice and review. We also thank Kristian Bartholdsson Frenander for insight into simulating aging. Lastly, we would like to give a huge thanks to our examiner Torbjörn Thiringer for the guidance and support during our thesis work.

We also thank Lena Sommarström for all the guidance and help over the years here at Chalmers and a large thank you goes out to Alva Lindström for help with the illustrations.

Felix Gråhn & Jakob Hogander
Gothenburg, April 2025

List of Acronyms

Below is the list of acronyms that have been used throughout this thesis listed in alphabetical order:

BEV	Battery Electric Vehicle
BES	Battery Energy Storage
BMS	Battery Management System
BTMS	Battery Thermal Management System
DFN	Doyle Fuller Newman
ECM	Equivalent Circuit Model
EV	Electric Vehicle
HEV	Hybrid Electric Vehicle
OCV	Open Source Voltage
ODE	Ordinary Differential Equation
P2D	Pseudo Two Dimensional
PDE	Partial Differential Equation
PI	Proportional-Integral
R-C	Resistance-Capacitance
SEI	Solid Electrolyte Interface
SOC	State of Charge
SOH	State of Health
SPM	Single Particle Model
SPMe	Single Particle Model With Electrolyte

Nomenclature

Below is the nomenclature of indices, sets, parameters, and variables that have been used throughout this thesis.

Indices

e	Electrolyte
j	Number index
k	Battery cell component index
n	Negative electrode
p	Positive electrode
s	Solid electrode
t	Terminal

Parameters

A	Area
a	Specific interfacial area
α_a	Anode charge transfer coefficient
α_c	Cathode charge transfer coefficient
b	Bruggeman coefficient
C_j	Capacitance at resistance capacitance pair j
C_{bat}	Battery capacity
D	Diffusion coefficient
F	Faraday's constant
h	Heat transfer coefficient
i_0	Exchange current density
η_s	Over potential

ϵ	Active material volume fraction
γ	Ration of lithium concentration
κ	Electrolyte phase ionic conductivity
L_k	Thickness of component
R	Universal gas constant
R_f	Solid-electrolyte interface layer film resistance
R_j	Resistance at resistance capacitance pair j
r_{eff}	Reaction rate constant
ρ_{eff}	Effective volumetric heat capacity
σ	The solid phase conductivity
T	Temperature
t_a^0	Transference number of the anion

Variables

$c_e(x,t)$	Lithium ion concentration in the electrolyte
$c_s(x,r,t)$	Lithium ion concentration of the active material
$i_e(x,t)$	Ionic current in the electrolyte
$j_n(x,t)$	Molar ion fluxes between the active material
N	Lithium flux within particles
Q	Total heat generation
Q_{cr}	Heating due to contact resistance
$Q_{Ohm,k}$	Ohmic heating
$Q_{rev,k}$	Reversible heating due to entropic change
$Q_{rxn,k}$	Heating due to electrochemical reactions
$\theta_e(x,t)$	Electric potential in the electrolyte
$\theta_s(x,t)$	Electric potential in the solid positive and negative electrode
r	Radial distance
t	Time step
x	Position

Contents

1

Introduction

With the rapid development within the automotive industry that is turning towards electric vehicles, there is always need for new technology constantly being developed to meet the needs of the market. Sales of electric vehicles in 2023 increased with 35% year-on-year to 14 million vehicles compared to 2022. The weekly sale of electric vehicles in 2023 was more than the annual sale ten years earlier in 2013, and there are no signs that this development is slowing down [1]. Climate change is a large driving factor for the rapid development of electric vehicles. Electric vehicles offer a distinct advantage compared to vehicles that use traditional combustion engines running on fossil fuels in that they have zero tailpipe emissions. The biggest climate impact occurs in an electric car life-cycle in the mining of materials and in production and the battery is an important contributor in this. This makes aging of battery cells an important factor in combating climate change, since the longer a battery is in use, the lower the impact on the climate.

The development of high-voltage battery systems for electric vehicles is a long process with many different subsystems that have to work together. Having the ability to accurately simulate the system in an early stage of the development process is important to be able to identify problems in the design early on. It also gives developers the ability to explore different solutions and configurations at a lower cost. The farther development goes from simulation to hardware testing, the more costly these projects will become.

The modeling of lithium-ion batteries has been researched for many years, and it has only increased as electric vehicles have taken up a larger market share. Many different models have been developed over the years to predict the behavior of batteries. The two main ways batteries are modeled are physics-based models or empirical models. These different models are suitable for different applications with their respective advantages and limitations.

The main focus of this project is physics-based modeling of lithium-ion battery packs used in electric vehicles. A hybrid approach using both empirical and physics-based models will be evaluated against models available today.

1.1 Previous research

There has been extensive research on the subject of modeling full-scale battery packs. This research has mainly been focused on modeling the battery pack with empirical models such as the equivalent circuit model rather than physics-based models such as the single particle model. The reason is that physics-based models are computationally heavy to run compared to empirical-based ones. On the scale of a full battery pack, the computational load often becomes too heavy to run. Research into creating a battery pack model with a lower computational load and still keeping the functionality of a physics-based model is where this thesis will aim to contribute. This is an area where current research is lacking.

1.2 Problem description

There is many factors that have to be taken into account when designing a method to model a full-scale battery pack, precision, robustness, simulation speed, and the ability to utilize the method for different battery packs. Since physics-based models are computationally heavy, empirical models are used more often for modeling on the pack level. This leads to a model that can give a simplified version of how the pack will behave, but many important aspects are lost. These models cannot give insight into the electrochemical parameters that are important in regard to performance and aging.

A solution to this could be to create a hybrid modeling method that has the capabilities of the physics-based models, but with a lower computational load. Using a combination of physics-based and empirical models leads to a trade of between accuracy and computational speed that has to be taken into account.

1.2.1 Scope

This project aims to create a method for modeling full-scale battery packs taking into account the physical aspects of battery cells but with a lower computational load compared to a fully physics-based model. To achieve this, a model will be built in Simulink with the addition of Simscape battery and PyBaMM. Investigation of other possible software to complete the goal will not be done, since this is software that is used by Volvo cars today and can be more easily integrated to their work today.

The model will be used to simulate use cases related to real-world battery pack customer scenarios. Fast charging simulations will be performed to evaluate the performance of the model. Comparison of the charging profile of the model to the charging profiles used today. The battery will be cycled to see the effects of aging on the battery pack of different kinds of driving and charging.

With the development of this model, methods will be developed to implement the model in other types of battery packs. Methods for this kind of modeling do not exist in the market and are something that could aid in the development of battery packs in the future.

1.2.2 Purpose

The purpose of this thesis is to evaluate whether a hybrid modeling method for full-scale battery packs is a viable solution to the trade-off between accuracy and computational speed. Comparison to existing models for battery packs and evaluation of how the approach can aid in the development of electric vehicles.

2
Theory

In the following chapter, all necessary theory to complete this master thesis will be presented.

2.1 Equivalent circuit model

The equivalent circuit model (ECM) is a widely used approach to model battery cells and estimate their state of charge (SOC). The ECM model uses the drawn current to model the battery behavior and predict the terminal voltage, V_t[2]. This model reduces the need for understanding the internal electrochemical mechanics of the battery and only requires a select few parameters[3]. Coulomb counting is first used to calculate the SOC[2]. Coulomb counting is a method where the total energy transferred through the battery is counted by measuring the input and output current continuously. This results in a measurement of ampere hours[4]. The equation used for this is

$$\frac{dSOC}{dt} = \frac{I}{C_{bat}} \tag{2.1}$$

where the current I is divided by the capacity of the battery C_{bat} and integrated over time. C_{bat} has the unit $(As)^2$. SOC is unitless and represents the amount of energy is stored in the battery and takes on a value between 0 and 1, witch is used to indicate 0-100%.To calculate the open circuit voltage (V_{oc}) a nonlinear function of the SOC is used[2].

The model uses a series of resistor-capacitor (R-C) pairs. The voltage of these are governed by

$$\frac{dV_{cj}}{dt} = -\frac{1}{R_j C_j} V_{cj} + \frac{I}{C_j} \tag{2.2}$$

where R_j and C_j denotes the resistance and capacitance in each pair. The model also includes the internal resistance of the battery cell, this is represented by R_0. The internal resistance is connected to the R-C pairs in series, as shown in Figure 2.1.

The final output of the model is the terminal voltage V_t. The terminal voltage is given by

$$V_t = V_{oc}(SOC) + \sum_{j}^{n} V_{cj} + IR_0 \tag{2.3}$$

this shows a sum of the open circuit voltage (OCV), V_{cj} and the voltage drop that is caused by the internal resistance of the cell R_0[2].

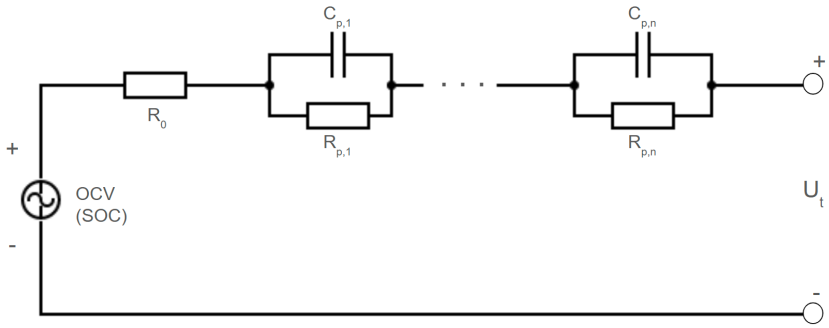

Figure 2.1: Visual representation of the Equivalent Circuit model, inspired by [5].

2.2 Physical based models

Lithium-ion batteries consist of a separator, an electrolyte, two electrodes, and two current collectors, as can be seen in figure 2.2.

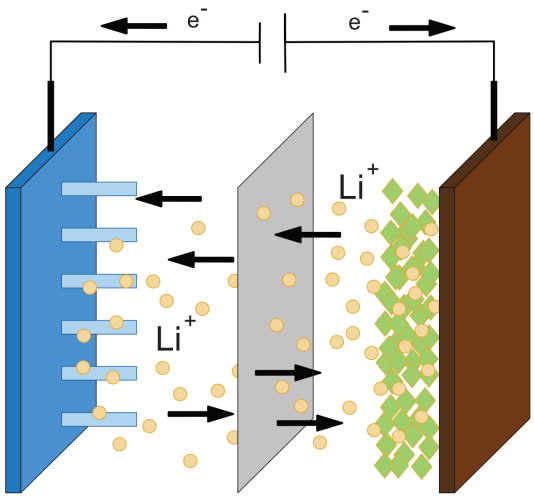

Figure 2.2: Lithium-ion battery diagram, inspired by [6].

This is a very simple way to represent a lithium-ion battery cell. Despite their relatively simple construction and few components, they can be difficult to model. There are many different ways to model battery cells. This thesis will mainly focus on physics-based lithium-ion battery models. Physics-based models depend on the use of governing equations to model the behavior of the battery[6].

In the following subsections, different physics based models will be introduced. Both their advantages and their shortcomings within different applications will be showcased.

2.2.1 Pseudo-two-dimensional model (P2D)

In 1993 Doyle et al. developed the Doyle-Fuller-Newman (DFN) model, which is the most common P2D model used today[6]. In that model, the electrodes are considered as porous matrices, and they are modeled as spherical particles surrounded by the electrolyte. A 1-D mathematical model can be applied since the battery transfer processes are mostly unidirectional. This creates a model that gives accurate modeling of a battery cell but is computationally heavy[7].

There are four important domains that are included in the P2D model. They are the two porous electrodes, the electrolyte and the separator. The reactions during charge and discharge are modeled within these domains[8]. A visual representation of the model is showed in Figure 2.3.

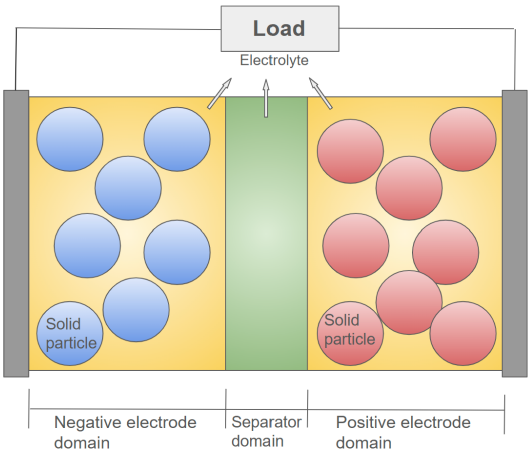

Figure 2.3: Visual representation of the Doyle-Fuller-Newman Pseudo-two-dimensional model, inspired by [8].

The electrochemical model then models these processes via six different state variables that are listed in table 2.1.

Table 2.1: State variables for electrochemical model

$\theta_s(x,t)$	Electric potential in the solid positive and negative electrode
$\theta_e(x,t)$	Electric potential in the electrolyte
$c_s(x,r,t)$	Lithium ion concentration of the active material
$c_e(x,t)$	Lithium ion concentration in the electrolyte
$i_e(x,t)$	Ionic current in the electrolyte
$j_n(x,t)$	Molar ion fluxes between the active material in the electrodes and electrolyte

The governing equations for the six state variables can be expressed as algebraic equations and partial differential equations (PDEs). With $i_e(x,t)$, the current in the cell I and the solid phase conductivity σ the potential in the solid electrode can be calculated with

$$\frac{\partial \theta_s(x,t)}{\partial x} = \frac{i_e(x,t) - I(t)}{\sigma} \tag{2.4}$$

The indices e and s indicate if it refers to the electrolyte or solid particles. The potential in the electrolyte is calculated as

$$\frac{\partial \theta_e(x,t)}{\partial x} = \frac{i_e(x,t)}{\kappa} + \frac{2RT}{F}(1-t_c^0)\left(1 + \frac{d\ln f_{c/a}}{d\ln c_e}(x,t)\frac{\partial c_e(x,t)}{\partial x}\right) \tag{2.5}$$

where R is the universal gas constant, T is the temperature and F is Faraday's constant, $f_{c/a}$ is the electrolyte active coefficient, κ is the electrolyte phase ionic conductivity, r is the radius and D_s is the solid phase lithium diffusion coefficient. The lithium-ion concentration in the solid particles c_s is calculated with

$$\frac{\partial c_s(x,r,t)}{\partial t} = \frac{1}{r^2}\frac{\partial}{\partial r}\left(D_s r^2 \frac{\partial c_s(x,r,t)}{\partial r}\right) \tag{2.6}$$

where r is the radial distance of the solid particles. The lithium ion concentration in the electrolyte can be calculated with

$$\frac{\partial c_e(x,t)}{\partial x} = \frac{\partial}{\partial x}\left(D_e \frac{\partial c_e(x,t)}{\partial x}\right) + \frac{1}{F\epsilon_e}\frac{\partial (t_a^0 i_e(x,t))}{\partial x} \tag{2.7}$$

where ϵ_e is the active material volume fraction for the electrolyte and t_a^0 is the transference number of the anion. The current in the electrolyte can be calculated as

$$\frac{\partial i_e(x,t)}{\partial x} = aFj_n(x,t) \tag{2.8}$$

where a is the specific interfacial area. The molar flux is given by the Butler-Volmer equation where η_s is the over potential and α_a,α_c is the charge transfer coefficients is calculated

$$j_n(x,t) = \frac{i_0(x,t)}{F}\left[\exp\left(\frac{\alpha_a F}{RT}\eta_s(x,t)\right) - \exp\left(\frac{-\alpha_c F}{RT}\eta_s(x,t)\right)\right] \tag{2.9}$$

where R_f is the resistance of the solid-electrolyte interphase layer film. The over potential η_s is calculated using

$$\eta_s(x,t) = \theta_s(x,t) - \theta_e(x,t) - U(c_{ss}(x,t)) - FR_f j_n(x,t) \tag{2.10}$$

where i_0 is the exchange current density and is calculated as

$$i_0(x,t) = r_{eff} c_e(x,t)^{\alpha_a}(c_{s,max} - c_{ss}(x,t))^{\alpha_a} c_{ss}(x,t)^{\alpha_s} \tag{2.11}$$

where r_eff is the reaction rate constant.

2.2.2 Single particle model (SPM)

The single particle model is based on the P2D model but with some assumptions about the cell to lower the computational burden while still getting accurate results. It is assumed that the current applied to the cell is small and that the conductivity of the electrolyte is very high [9]. The electrolyte concentration is assumed to be constant throughout the area. The current will not vary with the space within the electrolyte. The solid electrodes are also simplified down to just one positive and one negative particle. With these assumptions, the model can be simplified from five PDEs and one algebraic equation down to two PDEs and one algebraic equation. This is compared with the pseudo two dimensional model[8]. A visual presentation of the SPM is illustrated in Figure 2.4

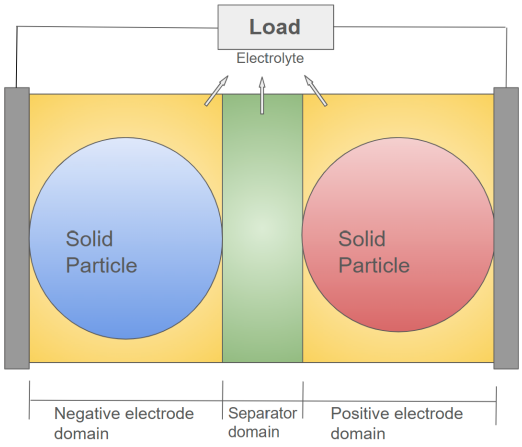

Figure 2.4: Visual representation of the single particle model, inspired by [8].

The PDEs needed to solve the SPM is to calculate the concentration of lithium-ions in the negative and positive solid electrode as

$$\frac{\partial c_s^{\pm}(r,t)}{\partial t} - \frac{1}{r^2}\frac{\partial}{\partial r}\left(D_s \frac{\partial c_s^{\pm}(r,t)}{\partial r}\right) = 0 \tag{2.12}$$

where $c_s^{\pm}$ is the lithium ion concentration of the solid particles. The algebraic equation for the terminal voltage is

$$V(t) = \theta_{s_0}^{+}(t) - \theta_{s_0}^{-}(t) - I(t)R_{collector} \tag{2.13}$$

This change reduces the computational load and the simulations are able to run faster than the one-dimensional electrochemical model[7].

2.2.3 Single particle model with Electrolyte (SPMe)

The single particle model with electrolyte is a model that, like the SPM, is a simplified DFN model. The main difference between the SPM model and the SPMe is that the SPMe takes into account the characteristics and concentration of the

electrolyte[10][11].

The model uses three main equations, two for the lithium concentration in the representative particles for the positive and negative electrode, respectively. These concentrations are indicated as $c_{s,p}$ and $c_{s,n}$. They are calculated according to

$$\frac{\partial c_{s,k}}{\partial t} = -\frac{1}{r_k^2}\frac{\partial}{\partial r_k}(r_k^2 N_{s,k}) \tag{2.14}$$

where r_k denotes the radial coordinate of either the positive or negative particle that represents the positive or negative electrode. The indices k is set as either n or p to denote whether it is the positive or negative particle. The indices s show that the parameter represents a solid electrode. $N_{s,k}$ is the flux of lithium ions within the particle and is calculated with

$$N_{s,k} = -D_{s,k}(c_{s,k})\frac{\partial c_{s,k}}{\partial r_k}, k \in n, p \tag{2.15}$$

The flux of the lithium ions in the solid particles have boundary conditions that are imposed on them. At the center the flux follows

$$N_{s,k}\Big|_{r_k=0} = 0, k \in n, p \tag{2.16}$$

At distance R_k which is at the surface of the particle the flux follows

$$N_{s,k}\Big|_{r_k=R_k} = \begin{cases} \frac{I}{Fa_n L_n}, & k = n, \\ \frac{I}{Fa_p L_p}, & k = p \end{cases} \tag{2.17}$$

L_k is the thickness and a_k is the particle radius R_k multiplied with and the surface area density.

The concentration in the electrolyte in the model is calculated with

$$\epsilon_k \frac{\partial c_{e,k}}{\partial t} = -\frac{\partial N_{e,k}}{\partial t} + \begin{cases} \frac{I}{RL_n}, & k = n \\ 0, & k = s \\ -\frac{I}{FL_p}, & k = p \end{cases} \tag{2.18}$$

D_e is the diffusion constant for the electrolyte. x represents the macroscopic distance and takes on a value between 0 and L. $N_{e,k}$ denotes the flux of lithium ions in the electrolyte and is calculated with

$$N_{e,k} = -\epsilon_k^b D_e \frac{\partial c_{e,k}}{\partial x} + \begin{cases} \frac{xt^+IRT}{FL_n}, & k = n \\ \frac{t^+IRT}{F}, & k = s \\ \frac{(1-x)t^+IRT}{FL_p}, & k = p \end{cases} \tag{2.19}$$

where t^+ is the transference number, ϵ_k is the volume fraction of the electrolyte and b is the Bruggeman coefficient.

The terminal voltage for the SPMe model is given by

$$V = U_{eq} + \eta_r + \eta_c + \Delta\Phi_{elec} + \Delta\Phi_{Solid} \tag{2.20}$$

where U_{eq} is the open circuit voltage. U_{eq} is calculated with

$$U_{eq} = U_p - U_n \tag{2.21}$$

where U_p and U_n is the potential of the positive and negative electrode. η_r represents the reaction overpotential and describes the voltage drop resulting from electrochemical reactions on the electrode surface. It is calculated by

$$\eta_r = -2sinh^{-1}\left(\frac{I}{j_{0,p}L_p}\right) - 2sinh^{-1}\left(\frac{I}{j_{0,n}L_n}\right) \tag{2.22}$$

The electrolyte concentration overpotential η_c is calculated with

$$\eta_c = 2(1-t^+)\frac{RT}{F}(c_{e,p} - c_{e,n}) \tag{2.23}$$

where $j_{0,p}$ and $j_{0,n}$ represent the electrode exchange current densities defined by

$$j_{0,p} = \frac{1}{L_n}\int_0^{L_n} \frac{\gamma_p}{\mathcal{C}_{r,p}}(c_p)^{1/2}(1-c_n)^{1/2}(1+\mathcal{C}_\urcorner c_{e,p})^{1/2}dx \tag{2.24}$$

$$j_{0,n} = \frac{1}{L_n}\int_0^{L_n} \frac{\gamma_n}{\mathcal{C}_{r,n}}(c_n)^{1/2}(1-c_p)^{1/2}(1+\mathcal{C}_e c_{e,n})^{1/2}dx \tag{2.25}$$

where γ_n and γ_p is the ratio of the maximum lithium concentration in solid electrodes, $\mathcal{C}_e$ is the ratio of electrolyte transport and discharge timescales, and $\mathcal{C}_{r,p}$ and $\mathcal{C}_{r,n}$ is the ratio of the reaction and discharge timescales[10].

$\Delta\Phi_{Elec}$ and $\Delta\Phi_{Solid}$ is the difference in the electrolyte and solid electrode potential. They are calculated with

$$\Delta\Phi_{Elec} = -\frac{\mathcal{C}_e I}{\gamma_e \kappa_e}\left(\frac{L_n}{3\epsilon_n^b} + \frac{L_s}{\epsilon_s^b} + \frac{L_p}{\epsilon_p^b}\right) \tag{2.26}$$

$$\Delta\Phi_{Solid} = -\frac{I}{3}\left(\frac{L_p}{\sigma_p} + \frac{L_n}{\sigma_n}\right) \tag{2.27}$$

where σ_n and σ_p represents the solid conductivity of the negative and positive electrode.

Thus, the SPMe consists of two PDEs for the concentration of both electrodes and one PDE for the concentration in the three regions of the electrolyte. The terminal voltage is calculated after solving the PDEs with an algebraic equation. This puts the computational load of the models higher than that of the SPM but lower than that of the full DFN model [10].

2.2.4 OKane2022 parameter set

O´Kane 2022 is a parameter set that is available within PyBaMM. This parameter set contains all necessary parameters that are needed to run the physics-based model in PyBaMM. O´Kane 2022 is set to represent the LGM50 battery cell. The parameter set is created by O´Kane et al[12]. That was based on the work of Chen et al.[13]. From the work of Chen et al. a parameter set called Chen2020 was created [12].

O´Kane sets itself apart from Chen2020 with its ability to simulate the aging of battery cells. Within the parameter set, several different aging mechanisms are implemented[14].

2.3 Battery degradation mechanisms

Battery cell degradation is an aspect that is a crucial part in the design of a high-voltage battery storage system. The degradation of battery cells leads to a decrease in performance over time, this decrease in performance is related to unwanted chemical reactions taking place within the battery. With the right system design and the use of a battery management system (BMS), these effects can be reduced, and therefore cells can be used for longer periods of time [15].

In the following subsections, different degradation mechanisms of battery cells will be introduced. The ways in which these mechanisms can be minimized will also be introduced. During this thesis, all modeling of aging will be done in PyBaMM.

2.3.1 Lithium plating

In lithium ion batteries there is an aging process called lithium plating, which means that a solid lithium deposit is created on the graphite anode[16].

This can be caused by the graphite anode being fully lithiated and surplus lithium having nowhere else to go. It can also be a result of high electrolyte potential during fast charging, which increases the amount of side reactions occurring within the cell. Moderate charge rates at below freezing temperatures can also cause lithium plating. Using the inverse reaction, lithium can be recovered from solid deposits. This is often referred to as stripping[17].

The chemical reaction that describes both stripping and plating is

$$Li^{+} + e^{-} \underset{\text{Stripping}}{\overset{\text{Plating}}{\rightleftharpoons}} Li(s) \tag{2.28}$$

(2.28) is given by [18].

Factors that accelerate lithium plating are high SOC, high charging current, high cell voltage, low temperatures, and lack of electrode mass or active surface area[19]. To negate the problem of insufficient mass and active surface area of the negative electrode, it is customary to include 10-20% of spare capacity[20].

2.3.2 Solid electrolyte interface layer growth

One consequence of lithium plating is that it can lead to other side reactions that impact cell performance. The metallic lithium that is formed reacts with the electrolyte to form solid electrolyte interface (SEI) growth. This growth can create dead lithium by electrically isolating the rest of the lithium. This process cannot be reversed. With this effect, lithium plating can be split into both reversible and non-reversible components[20].

This degradation mechanism contributes in different ways. The SEI growth on the negative anode contains lithium. This traps lithium in the SEI and makes it unable to contribute during charging and discharging. This is a concept that is referred to as loss of lithium inventory. The SEI growth also contributes to an increase of the internal resistance in the battery, reducing efficiency and power output[12].

2.4 Lithium ion-battery thermal characteristics

Lithium ion-batteries rely on electrochemical redox reactions within the battery to be able to be charged and discharged. During charge and discharge, heat is generated within the cell. This is caused by ohmic losses and exothermic reactions. An exothermic reaction is defined as a reaction in which the overall enthalpy change is negative. Within a module, the heat from cells affects other cells within the module via thermal coupling. This effect also expands to the neighboring modules and ends up affecting the entire pack.

During increases in rate of charge or discharge, the battery heat generation is increased, and as an effect the temperature of the battery pack increases. Having a battery operating at high temperature can be dangerous both for battery performance and passenger safety, since it can cause a thermal event or thermal runaway.[17].

The heat generation in cylindrical battery cells is observed at the center of the cylinder when looking in the radial direction. The heat is then distributed radially in the cells. The temperature spread within a cylindrical battery cell can be seen in Figure 2.5.

Heat generation within a battery cell can be described by

$$Q = -I(T\frac{dV_{oc}}{dT}) + I(V_{oc} - V_t) \tag{2.29}$$

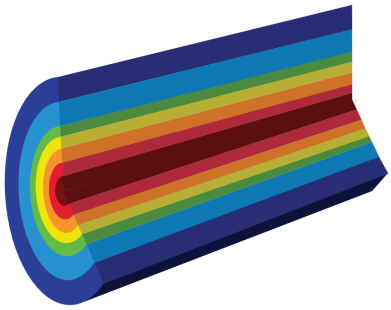

Figure 2.5: Spread of temperature within a cylindrical lithium ion-cell, inspired by [17].

(2.29) is given by [21]. I is negative during charge and positive during discharge, T is the temperature in kelvin, and $\frac{dV_{oc}}{dT}$ is the derivative of the OCV with aspect to temperature[22].

2.4.1 Battery thermal management system (BTMS)

During operation, heat generation within battery cells and in turn the battery pack is inevitable. If heat generation is left unmanaged it can lead to loss of capacity and in worst case to thermal runaway. Therefore, thermal management is a key aspect in battery pack design to be able to operate optimally [22].

In the current market, several different methods for thermal management are already available. Some examples of this are passive and active cooling, air cooling, liquid cooling, and solid-liquid change materials[22]. The following subsections will present air and liquid based cooling in more detail, since these are the most commonly used cooling methods used today[17].

2.4.1.1 Air based BTMS

Air cooling is generally divided into two types, passive and active cooling. Passive cooling as achieved by using the ambient air and letting it flow through the battery pack. In cases where the speed is not high enough or the ambient temperature is too high, active cooling is used. This is achieved by using additional convection to force more air through the battery pack and chill the air before it enters. Examples of active and passive cooling can be seen in figure 2.6 and figure 2.7.

Air cooling has both notable advantages and disadvantages compared to other methods of cooling a battery pack. When looking at advantages of air-based cooling, the weight of the cooling system is significantly lower than its counterparts. Since it

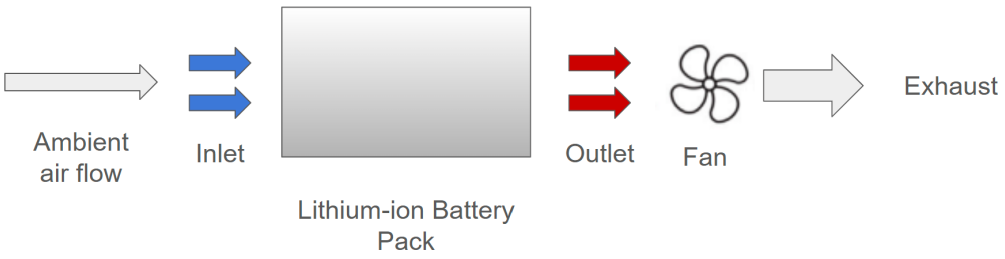

Figure 2.6: Natural Convection air based cooling, inspired by [17].

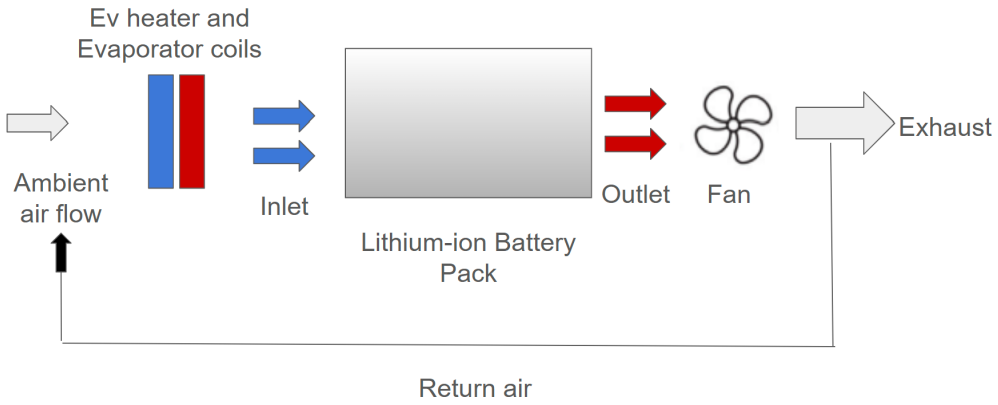

Figure 2.7: Forced convection air based cooling, inspired by [17].

requires few components, the weight can be kept low. Air-based cooling is also reliable and low maintenance when compared to other cooling methods[17].

The main disadvantages to air-based cooling is that it has a relatively low cooling power and the noise that is produces. This makes it less suitable for applications such as fast charge and high rate discharge. In these cases, air-based cooling simply does not have the power to keep the battery pack at the desired temperature.

Due to the aforementioned advantages and disadvantages, air-based cooling has to be used in the appropriate vehicle. When looking at the use of air-based cooling in the market now, it is mostly used for cheaper and smaller electric vehicles, hybrid electric vehicles (HEVs). These vehicles have less emphasis on the use of fast

charging and discharging. They generally also have smaller battery packs. All of this makes air cooling a great choice for these types of vehicles, since the cooling power needed is lower and the cost of the vehicle is kept down, since the cost of an air-based cooling system is lower[17].

2.4.1.2 Liquid based BTMS

Liquid cooling in EVs is generally separated into two categories, direct and indirect cooling. Indirect cooling is the most commonly used on the market today[23]. Indirect cooling systems utilize cooling plates or cylinders that channel liquid coolant. The cooled coolant enters these cooling plates and absorbs the heat from the battery cells that are in contact with the cooling plate. Then the coolant exits the cooling plate, is cooled down, and is sent through the cooling plate again[17].

In recent years, much research has been done on the subject of optimizing this cooling method. Several different cooling plate channeling designs have been used throughout the years. Examples of channeling design that are used is shown in figure 2.8.

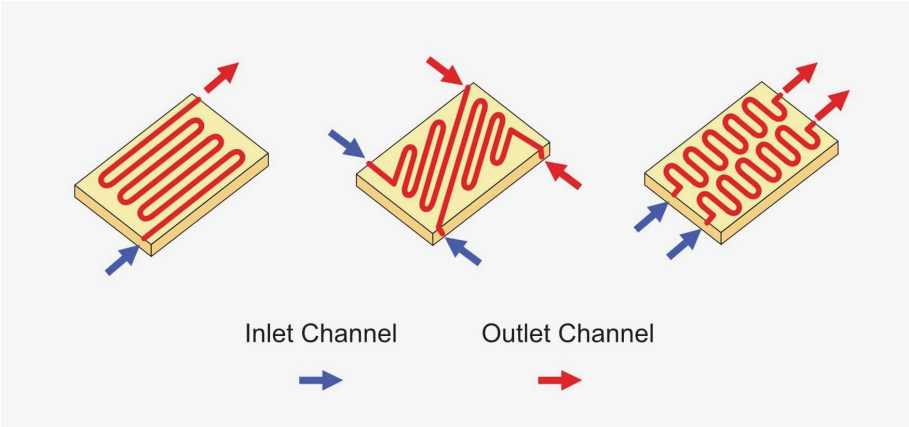

Figure 2.8: Cooling channeling configurations, inspired by [17].

There are many factors that go into designing these patterns. The channel dimensions such as hight and width, number of channels, and inlet flow rate. All of these contribute to the total heat transfer coefficient of the cooling plate[17].

Compared with air cooling, liquid cooling is a more complicated system. This leads to a higher cost and is more prone to the need for maintenance. The upside of using liquid-based cooling is that the cooling power is generally higher than that of air-based cooling[17].

2.5 Thermal modeling

The thermal modeling in this work will be done in both Simscape battery for the larger pack model and in PyBaMM for the monitors. The following subsections will

present how this modeling is done in both programs respectively.

2.5.1 Simscape thermal modeling

The modeling within Simscape battery is based on modeling a specific type of liquid cooling system. For this project, bottom plate cooling is used since it is the type of cooling that is used in the vehicles we are modeling. The heat exchange between the thermal mass and the cooling plate is calculated from

$$Q = KA\frac{dT}{dx} \tag{2.30}$$

where K is the plate thermal conductivity, T is the temperature and A and x denote the plate thickness and number of partitions[24].

2.5.2 PyBaMM thermal modeling

For the PyBaMM monitors the thermal modeling is done with a lumped model. The lumped model uses an ordinary differential equation (ODE) to calculate the temperature

$$\rho_{eff}\frac{\partial T}{\partial t} = \overline{Q} - \frac{hA}{V}(T - T_\infty) \tag{2.31}$$

where ρ_{eff} is the effective volumetric heat capacity, $\overline{Q}$ is the term of the averaged heat source, T_∞ is the ambient temperature, and V and A are the volume and area of the cell. There must be an initial temperature set that is represented by T_0[25].

The effective volumetric heat capacity is calculated with

$$\rho_{eff} = \frac{\sum_k \rho_k c_{p,k} L_k}{\sum_k L_k} \tag{2.32}$$

where ρ_k is the density, L_k is the thickness and $c_{p,k}$ is the specific heat. k is used as a subscript to denote the different components of the battery cell positive current collector, positive electrode, negative current collector, negative electrode and separator[25].

The heat source term Q represents all heat sources within the cell and is made up of several subheating sources. Q is made up of the heating from the contact resistance Q_{cr} that is calculated using

$$Q_{cr} = \frac{R_{cr}}{V_{cell}} i_k^2 \tag{2.33}$$

where R_{cr} represents the contact resistance, V_{cell} is the total cell voltage, and i_k is the current. Entropic change in the electrode $Q_{rev,k}$ is calculated using

$$Q_{rev,k} = a_k j_k T_k \frac{\partial U}{\partial T}\bigg|_{T=T_\infty} \tag{2.34}$$

where j_k is the current density and U is the open circuit potential. Irreversible heat from electrochemical reactions $Q_{rxn,k}$ is calculated with

$$Q_{rxn,k} = a_k j_k \eta_k \tag{2.35}$$

Ohmic heating $Q_{Ohm,k}$ is also taken into account and is calculated using

$$Q_{ohm,k} = -i_k \nabla \phi_k \tag{2.36}$$

where ϕ_k is the potential. k is used the same way as before to denote the different parts of the cell[25].

The total heat is then calculated using

$$Q = Q_{Ohm,k} + Q_{rxn,k} + Q_{rev,k} + Q_{cr} \tag{2.37}$$

$\overline{Q}$ is calculated by taking the volume average of Q[25].

3
Case setup

This chapter will present the methods that were used to obtain the results of the thesis work. To obtain the results, a simulation model that utilizes physics-based modeling needed to be built. This is to then be able to evaluate the results from the simulations coming from the new model.

3.1 Verification Model

To be able to verify the hybrid pack model, a validation model is built in Simulink. The input of a real test drive is inserted into the validation model, and then the output of the validation model is compared to the measured output data from the test drive. The input in the validation model is the current, the coolant temperature, and the coolant flow. In the validation model, different components can be implemented and tested before being implemented in the larger model. This ensures that the different additions to the model give accurate results.

The validation model uses ECM based modeling of the battery pack to reduce the computational load and increase simulation speed. Physics-based modeling was not needed for this model, since only the general trends and behaviors of the battery were studied. BTMS modeling was also included in the model. Creating the BTMS in this model made it possible to see that it was a good model as the temperature could be compared to the real test drive.

The outputs studied were voltage, temperature, SOC, and pressure in the cooling plate. As there is some measurement error in the equipment, some allowed errors were given for the model which can be seen in table 3.1.

Table 3.1: Acceptable errors in the model

Voltage	$\pm 20mV$
Temperature	$\pm 5K$
Pressure	$\pm 20kPa$

3.2 Simulation model

The model is built in Simulink with the Simscape add-on. Within the Simscape battery builder app, the battery pack was built with the exact dimensions and

number of cells, modules, and so on. The other main components of the model are the current controller and a PyBaMM cell that acts as a monitor of the battery pack.

3.2.1 Battery pack

The battery pack that was modeled is an 800 V pack meant for use in an electric vehicle. The energy of the pack is 104.8 kWh and the nominal capacity is 150 Ah. The cells used in the battery pack are LGM50 cells. There is a total of 5760 cells within the pack. The internal architecture of the pack is described in 3.2

Table 3.2: Internal architecture of the battery pack.

Section	Number of sub-sections
Pack	3 Modules assemblies
Module assembly	16 Modules
Module	12 parallel assemblies
Parallel assembly	10 cells

In figure 3.1 a visual representation of the battery pack from the Simscape battery builder can be seen. It also shows the simulation strategy used. All the modules were modeled as lumped to cut down on the computational load.

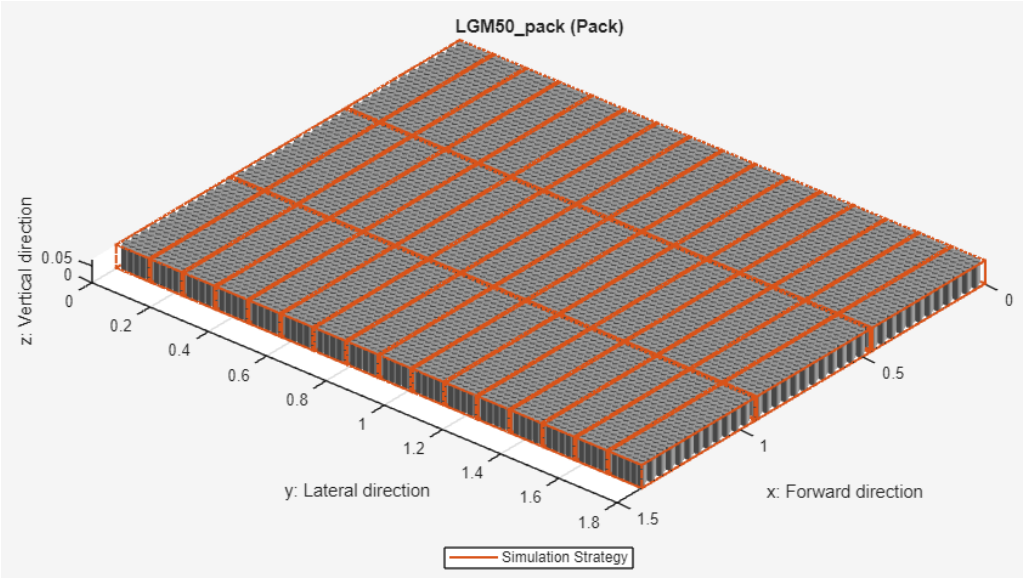

Figure 3.1: LGM50 pack configuration from Simscape Battery Builder

How the different components are connected can be seen in table 3.3. Where, for example, 10p12s means that the section consists of 10 subcomponents in parallel and 12 subcomponents in series.

Table 3.3: Connections between components in the LGM50 battery pack.

Section	Quantity	Configuration
Cells per module	120	10p12s
Modules per pack	48	3p16s

3.2.2 LGM50 cell

The cell used in this project is the LGM50 which is a cylindrical lithium -ion battery cell. The data for the cell can be seen in table 3.4. This is a well studied cell that is used in various research and the cell is also well parameterized [12][13]. There are also parameters set in PyBaMM based on the LGM50 cell making it a suitable choice of cell for the project.

Table 3.4: LGM50 cell parameters

Energy	18.20 Wh
Nominal capacity	5.0 Ah
Nominal Voltage	3.63 V
Maximum charge voltage	4.2 V
Weight	68.0 g
Diameter	21.10 mm
Height	70.15 mm

3.2.3 Thermal modeling

Within the simulation model, components will be implemented to model the thermal management of the battery pack. This will be done with existing thermal components in Simulink and Simscape. This will make it possible to see the thermal behavior of the cells and the battery pack as a whole.

The BTMS in the model consists of a liquid-based cooling system with a cooling plate. The cooling plate is located at the bottom of the battery pack, with U-shaped channels. The specific parameters of the cooling plate can be seen in table 3.5. The BTMS has one thermal node for each of the modules, making it possible to monitor the temperature of each module separately.

Table 3.5: Cooling plate parameters

Number of thermal nodes	48
Number of partitions	41
Channel thickness	$19 \cdot 10^{-3}$ [m]
Partition width	$14.7 \cdot 10^{-3}$ [m]
Thickness of cooling plate material	$1 \cdot 10^{-3}$ [m]
Thermal conductivity	209 [W/m·K]
Density	2700 [kg/m^3]
Specific heat	898 [J/K·kg]

In table 3.6 the temperature set points for the simulations are shown, the coolant flow is starting when the battery reaches a temperature of 308 K.

Table 3.6: Temperature set points

Ambient temperature	293.15 [K]
Cooling Power	5000 [W]
Cooling flow rate	0.33 [kg/s]
Initial temperature of cooling plate and coolant fluid	300 [K]

3.2.4 Current controller

The control unit for the input current of the pack is an important part of the model as it allows for more realistic simulations of the battery pack behavior. The current controller in our model regulates the current based on different parameters. The input current to the controller is based on a power signal divided by the cell voltage to obtain a current. The power signal differs according to the use case that is modeled at the time. A simple schematic of how the current controller interacts with the rest of the model can be seen in figure 3.2.

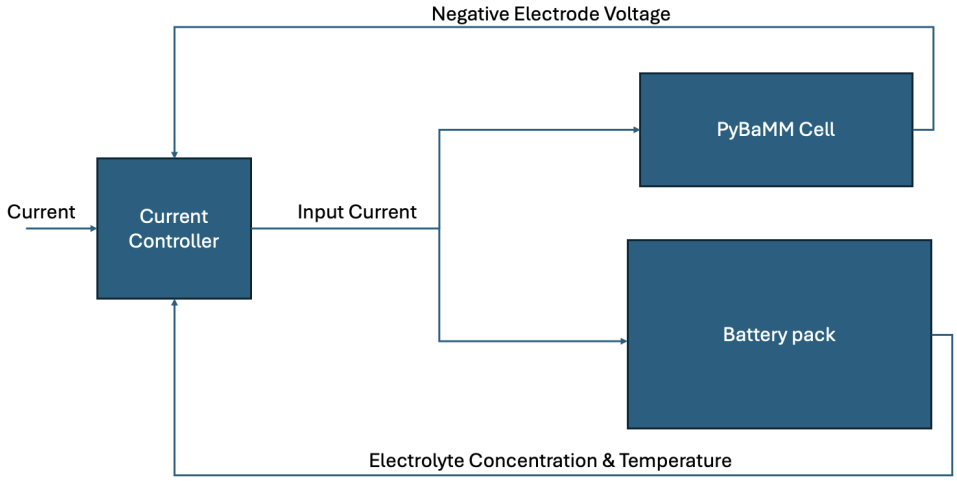

Figure 3.2: Block diagram of how the current controller is connected to other components in the model.

The current is regulated based on the negative electrode voltage. This is because during fast charge the negative electrode voltage drops drastically. If the negative electrode voltage drops below 0 it can result in lithium plating and in turn aging off the battery.

The anode electrolyte concentration is also taken into account in the current controller. The concentration is monitored by the SPMe modules in the Simscape pack.

Simscape splits the anode electrolyte concentration into 20 regions, and the measured region is the one closest to the current collector, as it reaches the lowest value during fast charge. The current controller makes sure that the concentration is kept above zero. This limit has to do with both reasonable results since the anode electrolyte concentration cannot go below zero in a real battery cell. This is mostly a problem when looking at high charge currents. During fast charging, the anode electrolyte concentration falls rapidly. The same is true for the cathode electrolyte during high discharge currents, so the current also needs to be regulated there.

The regulation of the current based on the anode electrolyte concentration and negative electrode voltage is done with proportional-integral controllers (PI-Controllers). Within the current controller, there are separate PI-controllers for each of the signals. The controllers use a proportional gain of 10 and an integral gain of 1.

The electrolyte concentration can also be seen from the PyBaMM cell, but from the PyBaMM model the output is the average electrolyte concentration. To obtain the lowest electrolyte concentration, the output needs to be from the SPMe module modeled by Simscape in the model, since the Simscape model allows the anode to be separated into shells. In this project the shell count is 20, leading to the anode electrolyte being seen in 20 instances correlating to the distance to the current collector, the same is true for the cathode.

The temperature of the battery cells is also taken into account when regulating the current. During high charge and discharge currents, the temperature of the cells will increase. The LGM50 battery cells should not exceed 60°C during discharge and 45°C during charge[26]. Exceeding these limits can lead to accelerated aging, or potential safety hazards. The temperature impacts the current through a Simulink current controller. This current limiter is activated when the pack temperature exceeds 323.15 K or 50°C. The current limiter will then gradually limit the current to 0 A if the battery reaches a temperature of 333.15K or 60°C.

3.2.5 PyBaMM model

PyBaMM will provide the model with the physical-based modeling of a battery cell. The PyBaMM monitors are integrated into Simulink and will be connected to the larger Simscape battery pack. This means that the output from the PyBaMM block is used as inputs for the battery pack. Investigations from Volvo Cars and MathWorks have concluded that PyBaMM is not able to integrate directly into Simscape. So, this is a method to integrate PyBaMM into a larger battery pack within Simscape.

The PyBaMM model can be customized with different settings to be able to simulate different parameters that affect the performance of a battery, the options used in the model are seen in figure 3.3

```
options = {"SEI": "solvent-diffusion limited",
"SEI porosity change": "true",
"lithium plating": "partially reversible",
"lithium plating porosity change": "true",
"particle mechanics": ("swelling and cracking", "swelling only"),
"SEI on cracks": "true",
"loss of active material": "stress-driven",
"thermal": "lumped"}
```

Figure 3.3: Used options in the PyBaMM cell related to aging and thermal

In PyBaMM, the lithium plating setting was set to partially reversible. This was chosen to give the model the most realistic behavior, as lithium plating in real batteries is partially reversible. Mechanical degradation mechanisms were also active in the cell with both swelling and cracking of the electrodes. These behaviors create a larger surface area of the electrode that can be affected by lithium plating. Stress-driven loss of active material was also active during simulations, making it possible to evaluate loss of capacity over time[27].

3.2.6 Battery aging modeling

The aging of the cells within the battery pack is an important part of the project and will also be included in the model. Aging will be modeled using the PyBaMM model. There are several aging mechanisms in the PyBaMM model that will be integrated in the model.

This is a great advantage of using a PyBaMM cell as a monitor, since Simscape itself cannot model aging. The PyBaMM model takes SEI growth and lithium plating into account when simulating. The PyBaMM setting related to aging can be seen in figure 3.3.

3.3 Use cases

This project will look at two use cases for the model. One will be used to look at the performance of the model and the other to be able to look at the aging mechanisms of the model. The following subsections will take a closer look at these use cases.

3.3.1 Performance, fast charging

The fast charging use case is conducted to be able to asses the performance of the model. The fast charging simulation is run from 10 % to 80 % SOC. This is because this is the range that fast charging is usually used in real EVs.

This input current to the model is based on a 350 kW fast charger. This value was chosen because it represents a typical fast charger available in the market. The

power is then scaled down to the per-cell power when entering the current controller of the model. The current is then controlled with the current controlled system during the entirety of the charge.

3.3.2 Fast charging at different initial temperatures

The fast charge model was tested to see how it could handle different initial temperatures of the battery. Fast charging at low initial temperatures can severley impact performance and simulation time. To run the tests the initial temperature of the pack was set to different values that can be seen in table 3.7.

Table 3.7: Initial temperature of the battery pack before fast charge

Temperature [K]
263 °K
273 °K
298 °K
315 °K

The ambient temperature was kept the same as the earlier fast charging test at 293.15 K, the cooling model was also kept identical to earlier tests. Like the original fast charging test the initial SOC was set to 10% and terminated at 80%.

3.3.3 Fast charging with aged cells

The behavior of an aged cell is different compared to a new one in 100% SOH. To be able to evaluate how the model acts with aged cells, a parameter that was changed was the initial inner SEI growth. As SEI growth is one of the major reasons for the aging of a battery cell, in figure 3.4 the loss of capacity can be seen with respect to the SEI growth of a cell. The inner SEI growth in PyBaMM refers to the SEI layer that forms directly at the interface of the anode and the electrolyte. The inner SEI growth contributes greatly to capacity loss and was thus chosen for these tests.

The test on the aged cell values from figure 3.4 will be used. This test looks at a cell with SEI growth corresponding to approximately 20%, 30% and 50% loss of capacity.

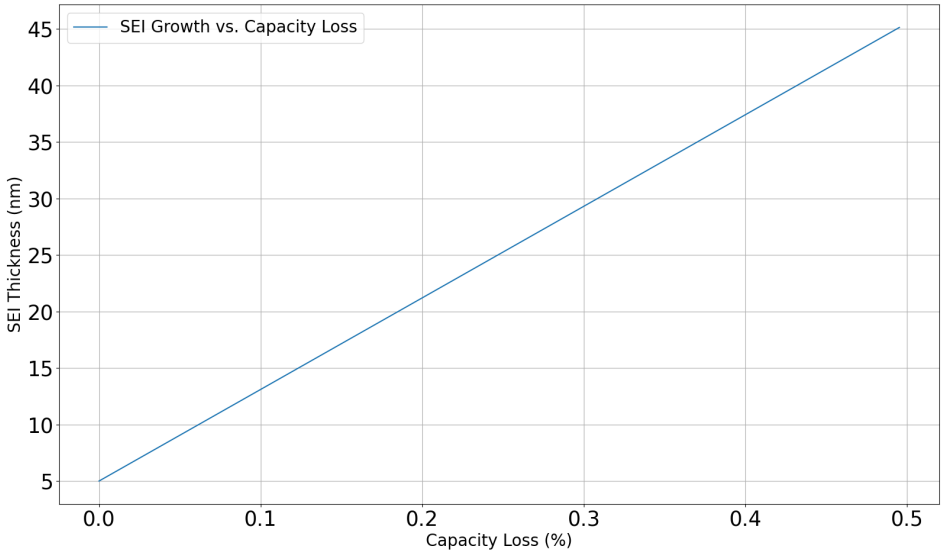

Figure 3.4: Change in SEI growth affecting Capacity loss of the battery cell modeled in PyBaMM

With these tests, it is possible to evaluate whether the fast charging model can handle aged cells.

3.3.4 Fast charging with Volvo Cars automotive cell

To be able to evaluate the fast charging model and how well the current controller performed, simulations based on Volvo battery cells were also done in addition to the LGM50 cell. The reason for doing this is so that the developed fast charging model could be compared to the Volvo fast charging protocol that is used today. In doing this, both charging time and risk for lithium plating could be evaluated for the respective fast charging strategies.

Due to the limited parametrization of the cell to be used in the PyBaMM monitor that is available today, the current is not controlled on the basis of temperature and anode electrolyte concentration. To be able to use the full current controller developed in this project, more parametrization is needed. As a result of these limitations, the simulations in this case are run at a constant temperature.

The cell has not been parametrized to be able to model aging either, so no analysis could be done on the Volvo cell.

3.3.5 Aging, cycling

The cycling of the battery is based on a combination of the fast charging model from the previous use case and the use of driving data to discharge the battery. The

Driving data was collected from a test drive on the autobahn conducted by Volvo cars. This data represents a power profile from a driving discharge.

The cycling of the battery is conducted with a control system that charges the battery pack with the fast charging current up to a given SOC. The input current is then switched to the driving input current from the test drive. When the SOC is discharged to a given value, the control system inputs the fast charging current again.

When the battery was cycled, going from fast charge to discharge, the Simscape pack was set up with only one SPMe module to reduce computational load and speed up the simulation time, but to still be able to control on the basis of the anode electrolyte concentration and negative electrode voltage, the PyBaMM monitors were still active in the model. They were chosen for the physics-based modeling since they have a lower computational load.

When running the aging modeling in PyBaMM it can be difficult to differentiate between reversible and irreversible lithium plating. So to be able to quantify the total amount of lithium plating a quantitative method to measure total lithium plate had to be implemented. To do this an integrator was implemented into the model, it was set up to integrate the negative electrode voltage under zero and add up all times the negative electrode voltage went below zero.

4

Results

4.1 Hybrid Model

The hybrid model of an electric vehicle battery was built using a mix of ECM modules and SPMe modules in the Simscape pack, as well as using two SPMe PyBaMM models as an external monitor, one ideal and one with the options that can be seen in figure 3.3.

4.2 Simulation speed

The simulation run-time has been of interest in this thesis work. During simulations that have been run with the model, the simulation time varies substantially based on the pack configurations. The computer that has been used to run these simulations is an HP Elitebook 840 G10, with a 13th gen Intel i7-1365U processor and 32 GB RAM running Windows 10 enterprise.

4.2.1 Physics based modules

Running the simulation with the pack configured with only ECM modeling. The simulation ran at a speed of approximately two seconds simulated per second. When one module per string was replaced with an SPMe module, the simulation slowed down significantly. The simulation then ran at approximately 1 second simulated per 1.6 seconds. This is caused by the increased computational load of the SPMe modules. At this simulation speed, the model was still usable.

Simulations were conducted in which more SPMe based modules were added. The simulation is expected to slow down when more physics-based modules are added. The results of these tests can be seen in table 4.1. From table 4.1 it can clearly be seen that this is the case. This leads to a trade-off between simulation speed and result accuracy that has to be taken into account when using the model. In all of these simulations, one PyBaMM monitor cell has been utilized in the model.

Table 4.1: Simulation run times with varying number of physics based modules.

Number of SPMe modules	Simulation time for one second simulated
0 modules	0.6 sec
3 modules	1.6 sec
6 modules	2.5 sec
7 modules	3.6 sec
8 modules	4.5 sec
9 modules	5.2 sec
11 modules	7.4 sec
13 modules	9.7 sec
15 modules	12.4 sec

4.2.2 Simulation strategy

In the aforementioned tests, all modules were modeled as lumped. This means that Simscape looks at the modules as one large cell. This makes it so that the model does not have to make individual simulations and calculations for each and every cell in the battery pack. This is a method used to lower the computational load of the model. The different simulation strategies can be seen in figure 4.1.

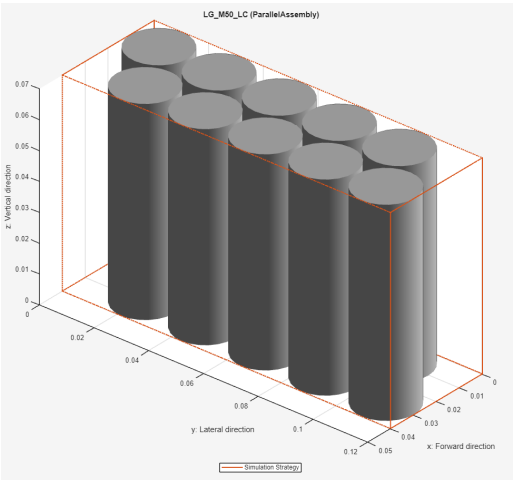

(a) Visual representation of lumped simulation strategy.

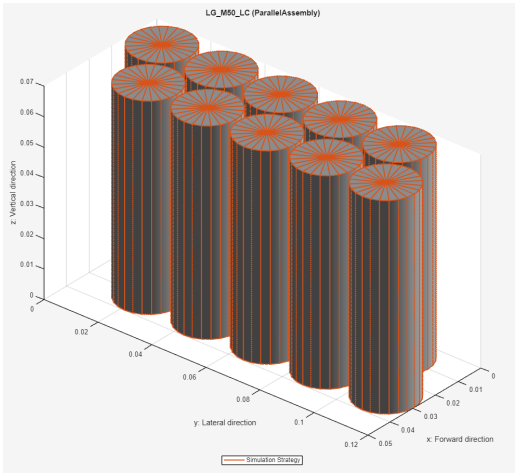

(b) Visual representation of detailed simulation strategy.

Figure 4.1: Simulation strategies visualization of a parallel assembly. Figures are taken from Simscape battery builder.

It was also investigated how the pack could be further discretized, by making individual cells into SPMe cells. Two tests were performed with one using 120 detailed SPMe cells and another with 10 detailed SPMe cells. In both cases the model was able to compile but not run due to the RAM memory running out.

4.2.3 PyBaMM cells

Simulations where also done with more than one PyBaMM cell in the model. This did not significantly impact the simulation speed. Adding an additional PyBaMM cell added approximately 4% to the simulation time.

4.3 Use cases

In the following subsections, the results from the different use cases for the model will be presented. The use cases were run to be able to evaluate the performance and limitations of the model.

4.3.1 Fast charge

In the fast charge case, the Simscape pack consisted of 1 SPMe module per parallel row of modules, which meant that the pack contained 3 SPMe modules and 45 ECM modules. Two PyBaMM monitors were also active during the fast charging simulations to be able to model an ideal cell and a cell that models aging aging effects as well. As fast charging protocols in electric vehicles are typically used up to 80% SOC, the simulation was terminated when 80% SOC was obtained. The initial SOC of the pack before fast charge was 10% during all simulations. It could also be observed that when simulating with fast charging currents above 80% SOC the cut-off voltage was reached before the battery reached 100% SOC. This is a limitation with the current controller, as when the SOC goes above 80% other parameters than the anode potential and the temperature affects the desired current magnitude.

In the first tests, the initial temperature of the pack and the PyBaMM cells were set to 298.15 K, as when looking at existing fast charge protocols it is outputting max current at that temperature, while below that temperature the energy is going to heating of the battery instead of charging.

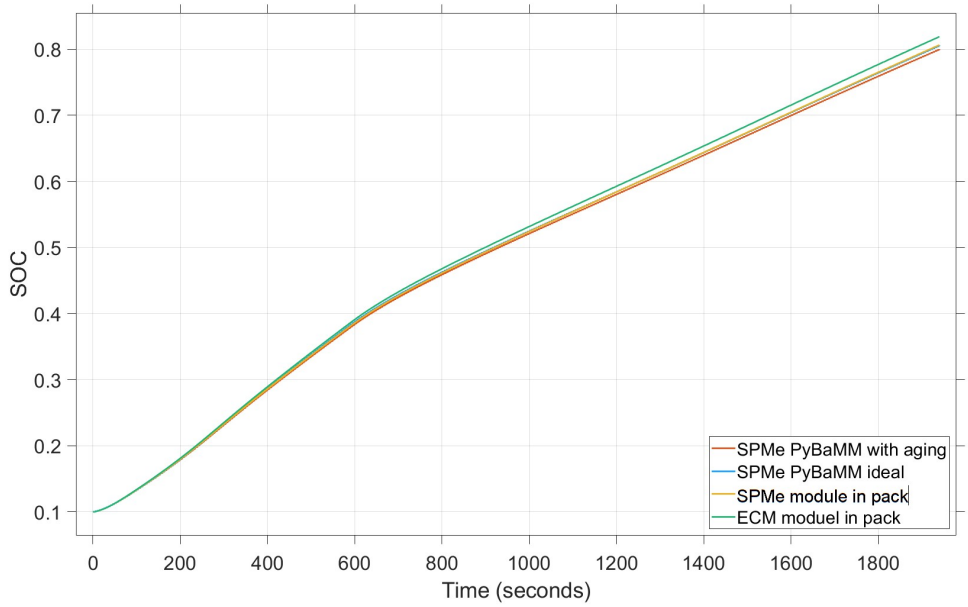

Figure 4.2: SOC of the different modules during fast charge

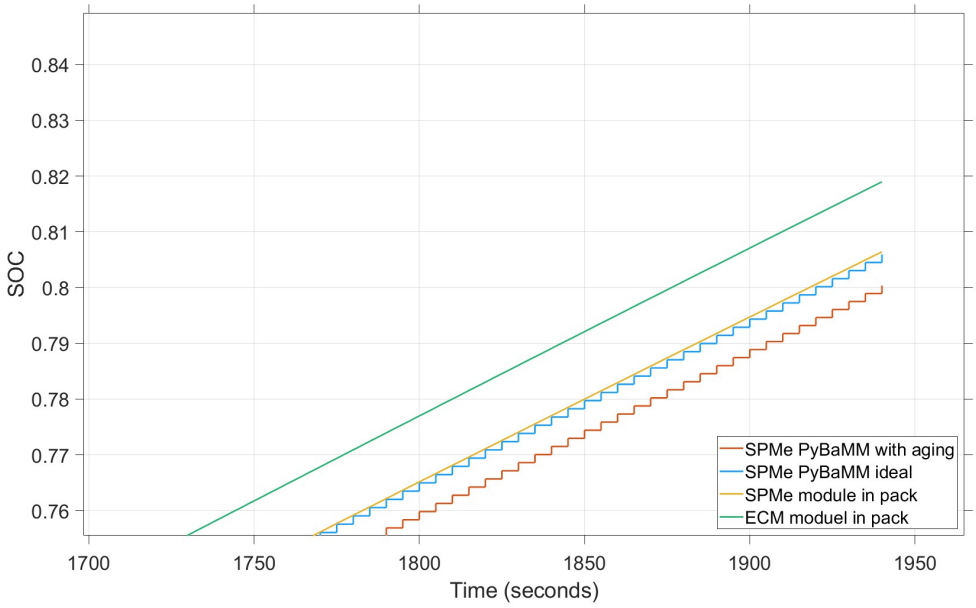

Figure 4.3: SOC of the different modules during fast charge from 75% SOC to 80% SOC.

From figure 4.2 it can be seen that the fast charge takes 1930 seconds or 32, 2 minutes. It can also be seen that the charge rate is reduced at around 35 % SOC. This is due to that the controller is lowering the charging current due to low anode concentration, this can be seen in figure 4.9. From the figure it can also be seen that all the physics based models, both PyBaMM and Simscape follow the same trend while the ECM model in Simscape is ahead during the later parts of the charge.

This is likely due to the simplifications of internal electrochemical dynamics. These dynamics can limit the batteries ability to charge at higher rates and thus ignoring them can lead to an over estimation of charging performance. Although it is a little ahead, it is by a very small margin. This can be seen in figure 4.3, the stop condition at 80% SOC is controlled by the PyBaMM cell with aging.

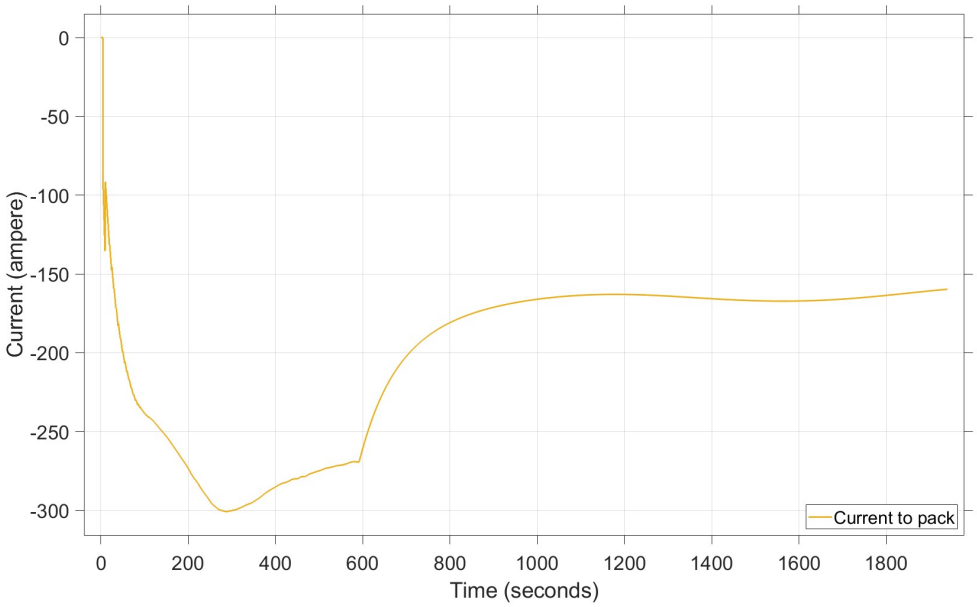

(a) Fast charge current to pack

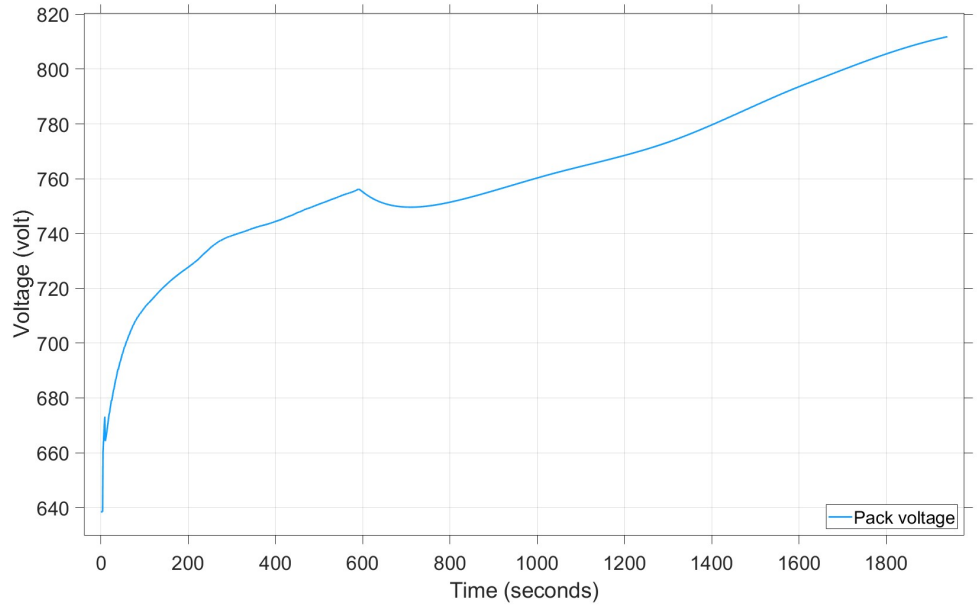

(b) Pack voltage

Figure 4.4: Current and voltage in the pack during fast charge from 10% to 80%

The fast charge current to pack profile can be seen in figure 4.4a. This current profile

is based on the internal electrochemical mechanisms of the battery with the help of the current controller. When either the negative electrode voltage or the anode electrolyte concentration is approaching zero, the current will cut out to counteract this and then resume when the value has risen again. This current profile is very different from the commonly used step-down current curve. The step-down current curve used for most fast charging today is based on extensive testing and not the real-time behavior of the battery.

In figure 4.4 the pack voltage can be seen. Here the same oscillations occur in the voltage as in the current this is also an effect of the current controller.

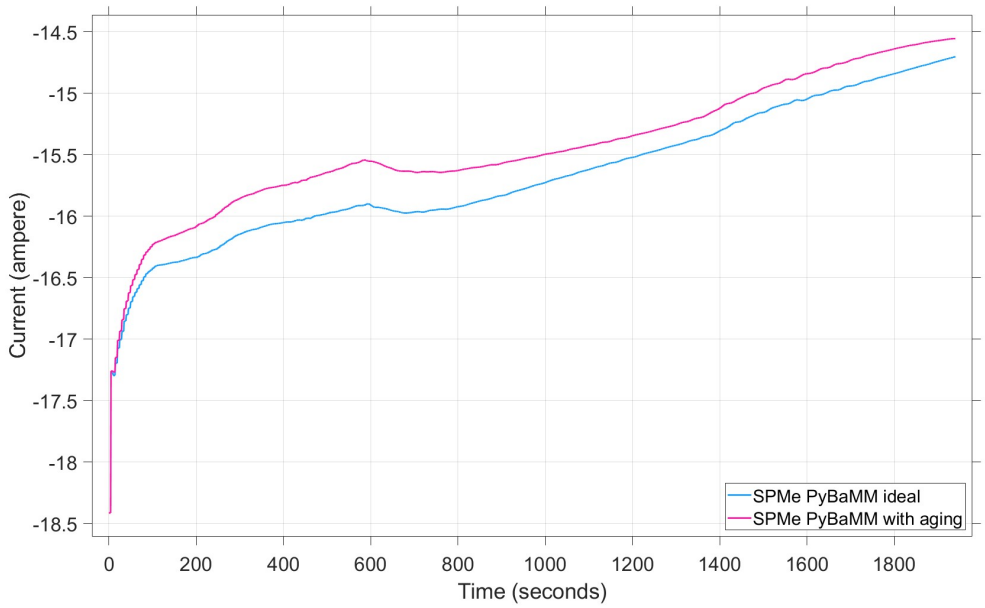

Figure 4.5: Current before the current controller for the two PyBaMM cells

In figure 4.5 the current profile to the PyBaMM cells before the current controller can be seen, where it can be seen that the PyBaMM model with aging options has a higher current. This is caused by the current being based on the terminal voltage that the fast charging power is divided by. The cell voltages of both PyBaMM cells can be seen in figure 4.7. This leads to a the PyBaMM cell with the lower terminal voltage also having the higher current input. Figure 4.6 shows the current profile after the current controller, which is the input to the PyBaMM cell and the battery pack.

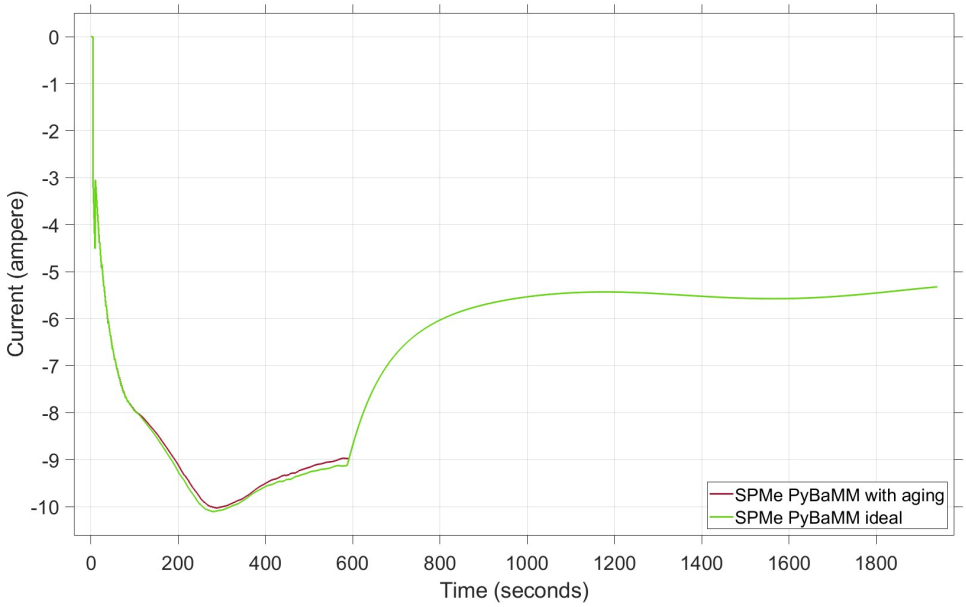

Figure 4.6: Current going into the two PyBaMM cells, after the current controller

Looking at the voltages of the fast charging simulation which can be seen in figure 4.7, it can be seen that the SPMe module of the battery pack performs similarly to the ideal PyBaMM cell, which correlates well with the pack modules, as neither SEI growth nor lithium plating is taken into account. The difference in voltage between the ideal PyBaMM cell and the PyBaMM cell with aging is on average 0.065 V during the whole simulation. Even with the discrepancies in voltage the SOC for the different modules are following each other. That is due to the voltage corresponding to a certain SOC is different depending on the settings of the module, but because of the current controller the current output to the different modules is the same leading to the SOC being the same for all modules.

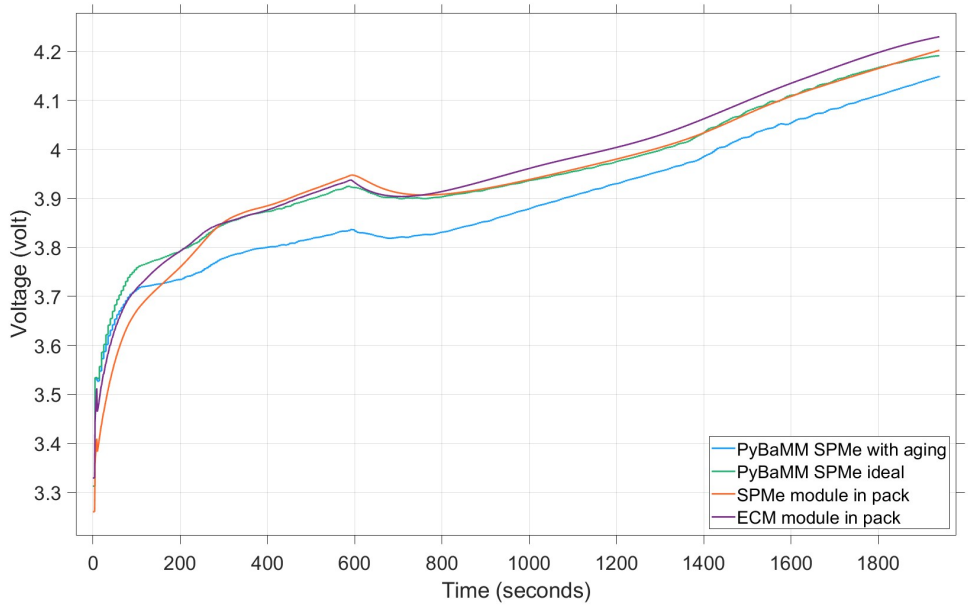

Figure 4.7: Voltages of the different modules during fast charging

The temperature of the different modules in the model during fast charge can be seen in figure 4.8. The temperatures differ a bit, the temperature difference between the SPMe and the ECM module is around 6 K when the steady state is reached, and because of that the PyBaMM cells are controlled with the average temperature from the pack, and thereby the temperature output from the PyBaMM cell is in between the ECM and SPMe module.

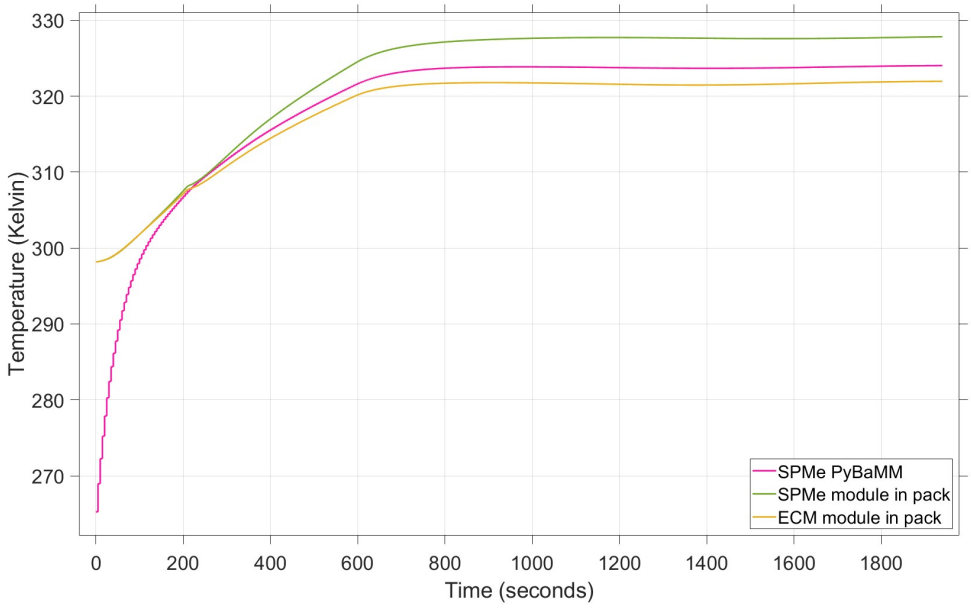

Figure 4.8: Temperature of the different modules during fast charge

In figure 4.9 the anode electrolyte concentration can be seen. Looking at the figure

it makes it clear why the current is acting in a certain way as a PI-controller in the current controller stops the anode electrolyte concentration from going below 0. This is taken from the part of the anode closest to the current collector as there the electrolyte concentration is the lowest. One limitation with the PyBaMM SPMe model is that the concentration output is the average, while in Simscape the concentration can be seen in different instances of the anode, meaning that the lowest concentration can be extracted from the battery and used for current control.

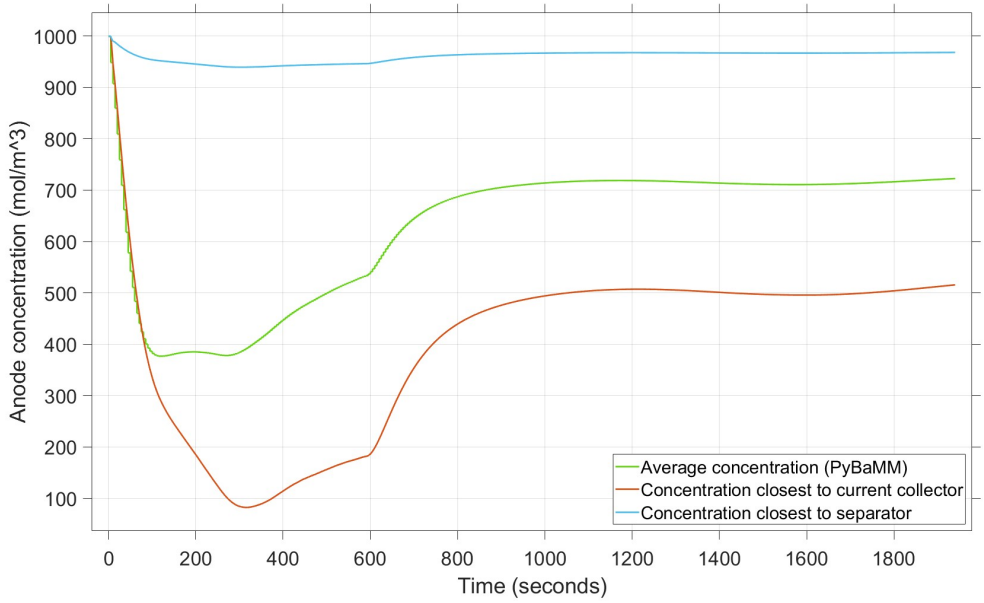

Figure 4.9: Anode electrolyte concentration in different sections of SPMe module in the battery pack and average concentration calculated by PyBaMM

Figure 4.10 shows the negative electrode voltage for the fast charge case. During high currents, the negative electrode voltages have the greatest risk to go below 0. It can be seen in figure 4.10 that the current controller manages to keep the negative electrode voltage above 0 even though it is very close when the charging current is at its highest.

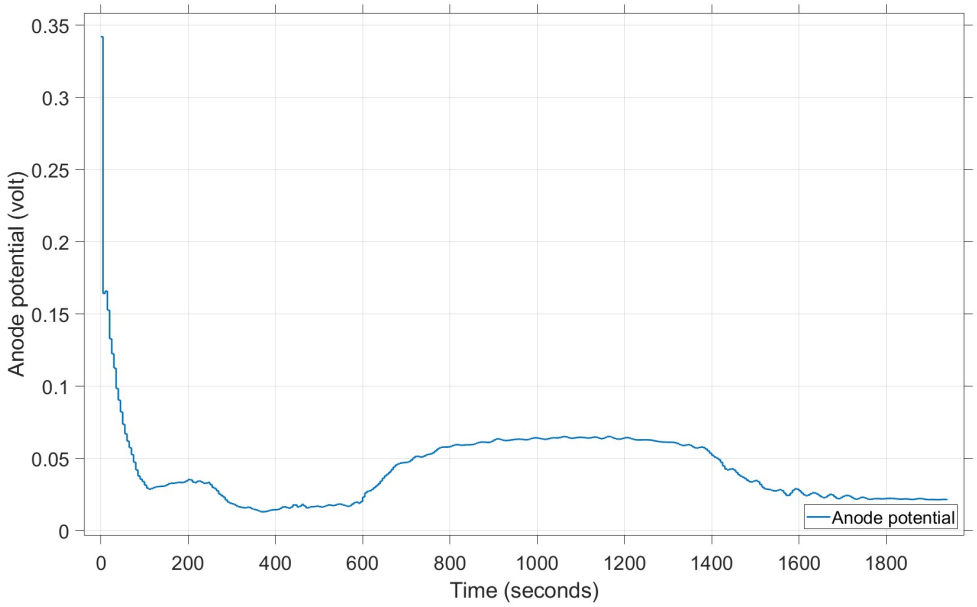

Figure 4.10: Anode potential during fast charge

From this simulation, it can be seen that the current controller works as intended. The temperature is kept within operating range for charging, and the negative electrode voltage is successfully regulated to keep it from going below zero, at the closest point the anode potential is at 13 mV. This shows that having the PyBaMM cell as a monitor made it possible to regulate on the basis of internal characteristics without having a fully physics-based model.

4.3.2 Fast charging with different initial temperatures

It is shown in figure 4.11 that the charging time from 10-80% SOC varies considerably between the different simulations with different initial temperatures. It can be seen that, when the temperature is lowered considerably, the charging time also increases notably, the charge times can be seen in table 4.2. This is an expected behavior since low temperatures generally decrease the charging performance of batteries. This is why in most electric vehicles the batteries are heated before charging. However, contrary to this trend, it can be seen that the battery with an initial temperature of 315 K charged slower than the battery at 298 K. This can be explained with the fact that the battery will increase even further in temperature during charging and then the current controller will step in and lowering the charging current, thus slowing down the charge.

Table 4.2: The difference in charge time between the different initial temperatures

Initial Temperature	Time to reach 80% SOC
263 K	3255 sec
273 K	2785 sec
298 K	1950 sec
315 K	2085 sec

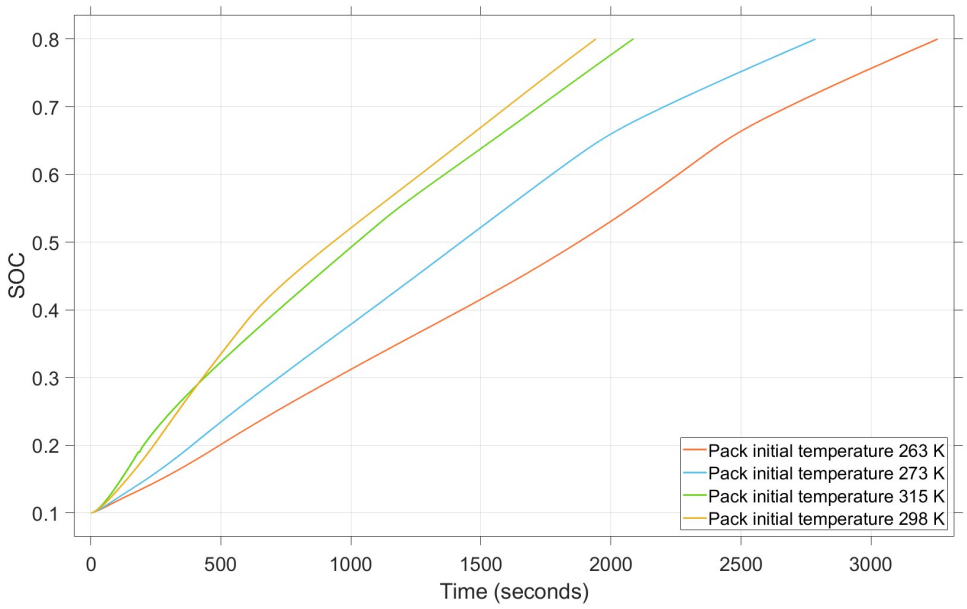

Figure 4.11: SOC profile of the battery pack with different initial temperatures

That the current controller limits the current of the pack starting at 315 K can be seen in the current profiles in figure 4.12. It can also be seen that the colder battery packs get a much lower charging current, slowing down the charge.

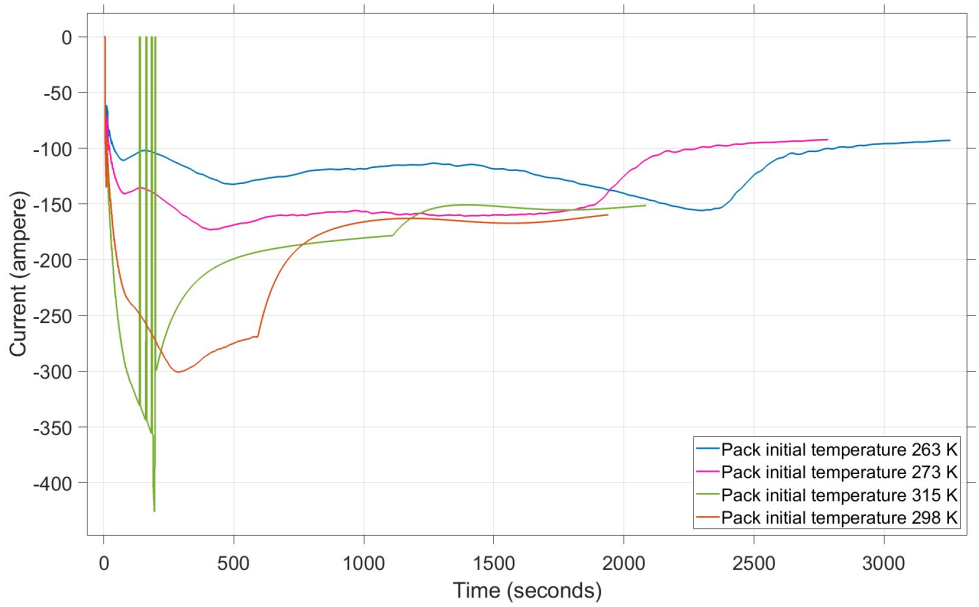

Figure 4.12: Pack current profile of the battery pack with different initial temperatures

The anode concentration closest to the current collector can be seen in figure 4.13, here it is clear that the higher charging currents in the battery packs with higher initial temperatures lower the anode concentration faster. It can be seen that in the case with an initial temperature of 315 K the concentration oscillates when is approaching zero, this is expected as the current controller is acting here.

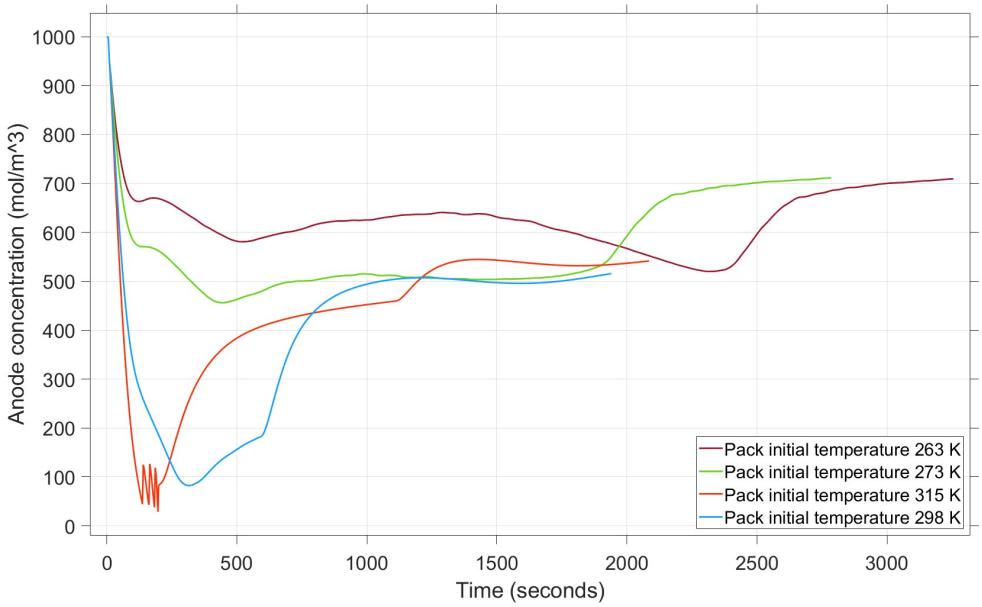

Figure 4.13: Anode concentration closest to the current collector of the battery with different initial temperatures

Looking at the anode potential that can be seen in figure 4.14, it can be seen that the controller is able to keep the potential over zero in all cases. The packs that started at a lower temperature have an anode potential that goes closer to zero during fast charge, this can be an effect of increased charge-transfer resistance as a result of the lower temperatures.

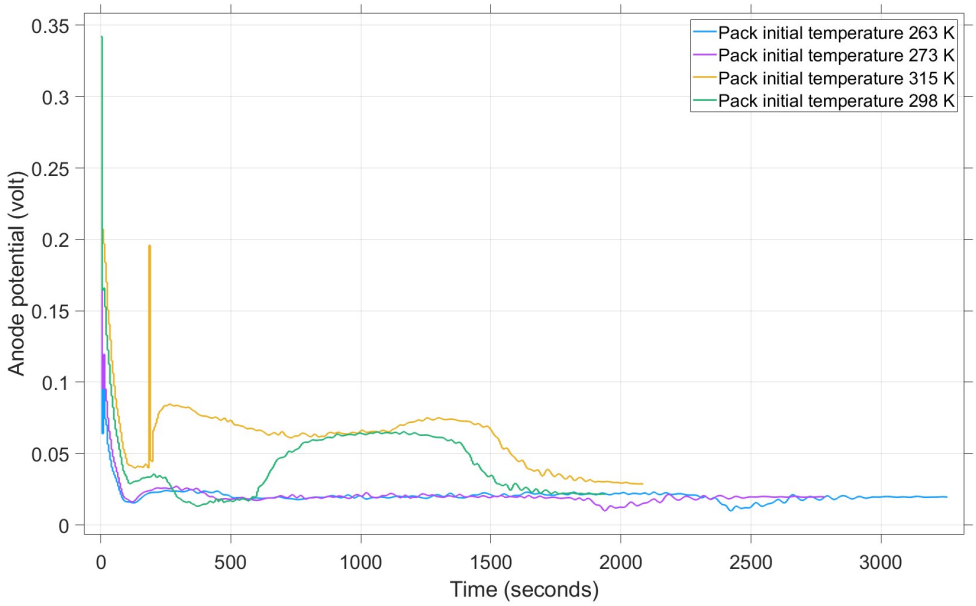

Figure 4.14: Anode potential of the battery pack with different initial temperatures

From this use case it was possible to see that the physics-based current controller could adjust to accommodate for different initial temperatures and not compromise on the aging risks of the pack. The differences in behavior between the different cases were also clearly visible in the results, which shows that the model can be used to evaluate the performance of a battery pack at different initial temperatures.

4.3.3 Fast charging with aged cells

The ability to model aging in the PyBaMM cell was used to simulate how the hybrid pack model worked with an aged battery. The initial inner SEI thickness was changed to correspond to a battery with a certain loss of capacity. In table 4.3 the set values for the initial thickness of the inner SEI growth can be seen.

Table 4.3: Capacity loss with regards to SEI thickness

Initial outer SEI thickness	Capacity loss
$25[nm]$	ca 20 %
$30[nm]$	ca 30 %
$45[nm]$	ca 50 %

During the simulations, the initial SOC of the battery pack was set to 10% SOC and the pack was charged to 80% SOC. The Simscape battery pack configuration was the same as the fast charging case with 3 SPMe based modules, one in each parallel row of modules and 45 ECM based modules. The current controller was used in these simulations as the fast charge use case. In figure 4.15 it can be seen that the packs with different amounts of capacity loss charged to 80% SOC in similar times. This can be seen in more detail in figure 4.16.

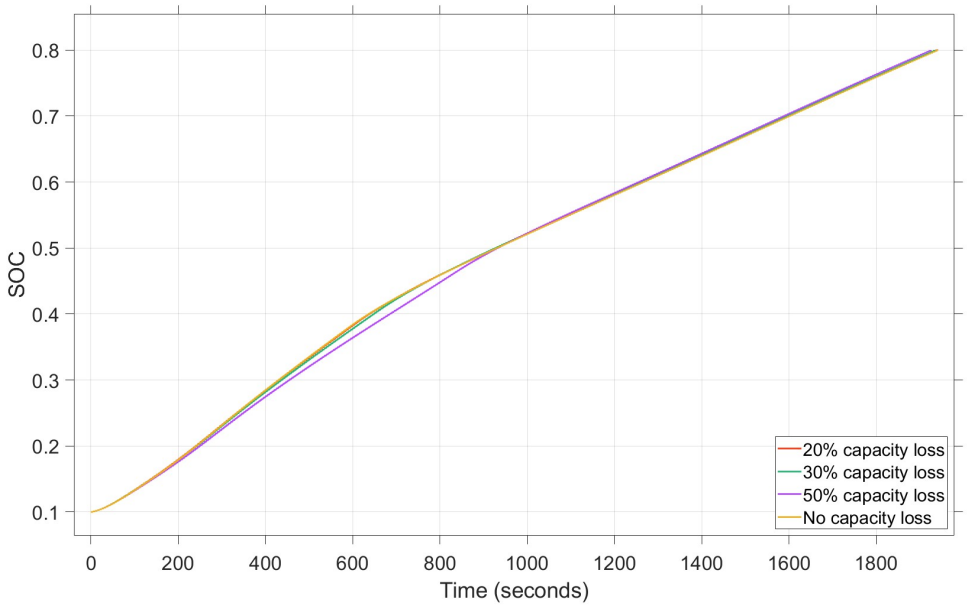

Figure 4.15: SOC during fast charge with different amounts of aging

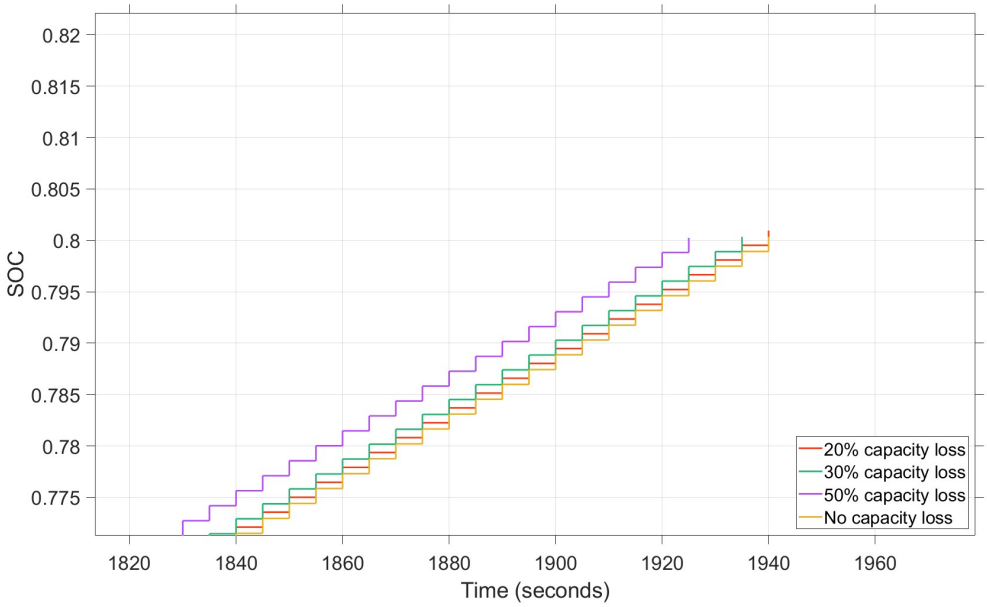

Figure 4.16: SOC during fast charge with different amounts of aging from 77% SOC to 80% SOC

In this case, the SOC of the pack is always calculated with the current capacity of the battery. So even if it can be seen that the aged cells charge to 80% SOC faster in figure 4.3, it is important to note that the total total energy charged is lower. So in the case of 50% capacity loss, the battery charges at roughly half the speed compared to the healthy pack. 80% SOC for the differently aged cells are recalculated based on the initial capacity and can be seen in table 4.4.

Table 4.4: Recalculated SOC based on initial capacity for aged cells

Capacity loss	**Aged cells 80% SOC recalculated with initial capacity**
20%	ca 64 % SOC
30%	ca 56 % SOC
50%	ca 40 % SOC

In figure 4.17 it is possible to see that the charging currents of the aged batteries are significantly lower than that of the 100% SOH battery. The increased internal resistance and the increased overpotentials in the aged batteries lead to a lower charging current with the same power input. Effects of this can also be seen in the voltage profile in figure 4.18. The voltage profiles of the batteries follow each other with small deviations. The peaks in the voltage profile for the batteries can be seen to match the sudden drops in the current due to the current controller.

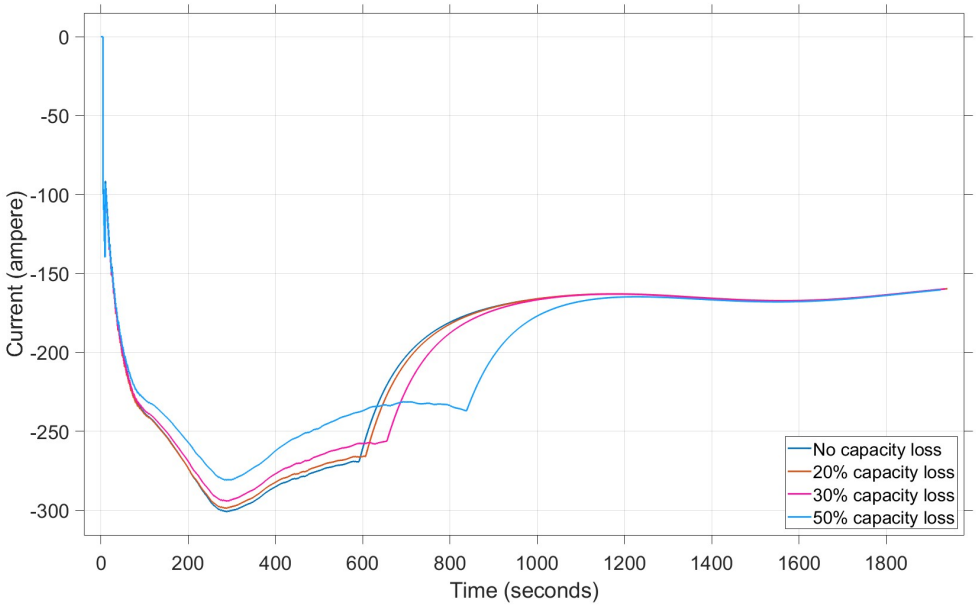

Figure 4.17: Current to pack profile during fast charge with different amounts of aging

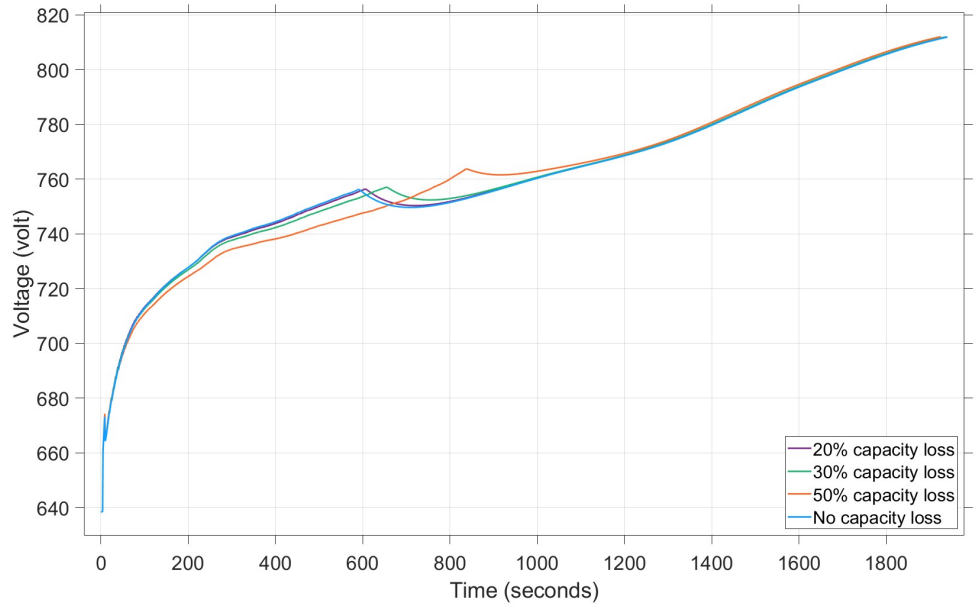

Figure 4.18: Pack voltage profile during fast charge with different amounts of aging

The anode potential profile of the batteries can be seen in figure 4.19, and the aged batteries can be seen to have a lower anode potential than the 100% SOH battery. The SEI growth causes a voltage drop that lowers the anode potential during fast charge. This results in the aged batteries being more prone to further aging compared to a fresh battery.

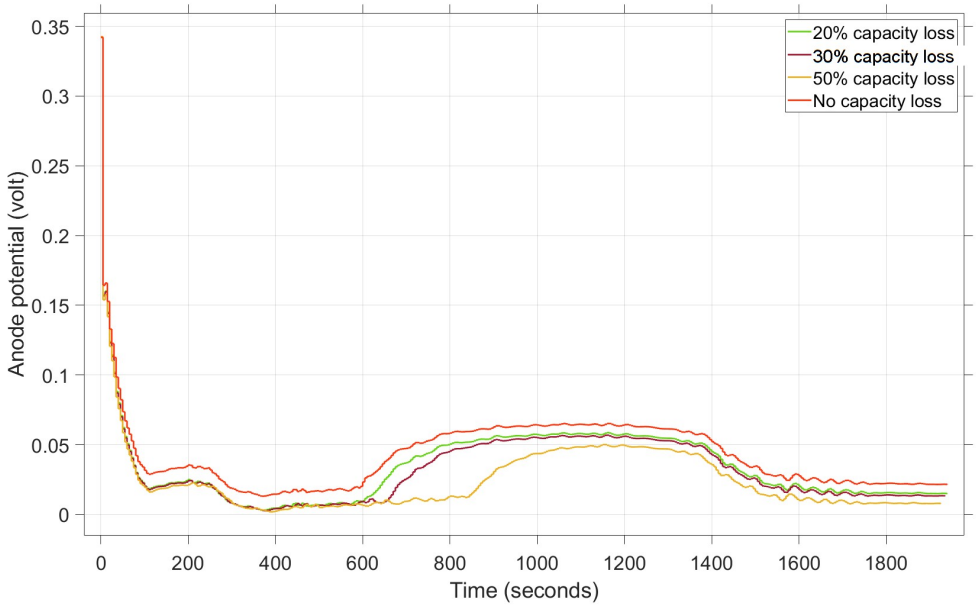

Figure 4.19: Anode potential profile during fast charge with different amounts of aging

These simulations show that the model can handle aged batteries during fast charge and that the effects of aging can be clearly seen in the results.

4.3.4 Fast charge with Volvo automotive cell

To test the model for a battery that is used in electric vehicles, a automotive cell from Volvo cars was used. In these simulations the Simscape battery pack only used ECM modeling for all modules in the pack and the PyBaMM cell used SPMe modeling. The Simscape pack used the fast charging protocol for current control while the PyBaMM cell used the physics-based current controller.

The current profiles can be seen in figure 4.20. The current to the ECM modules are based on the fast charging protocol that has been developed by Volvo cars and is whats used today. The current to the PyBaMM model is regulated based on the anode potential.

As the current in figure 4.20 is negative, the lower curve is at a higher current, meaning that the input current is higher for the case where it is controlled by the anode potential in the same way as the earlier fast charging simulations, at the largest difference in current magnitude during the simulation the current controlled by the physics-based controller is 75% larger.

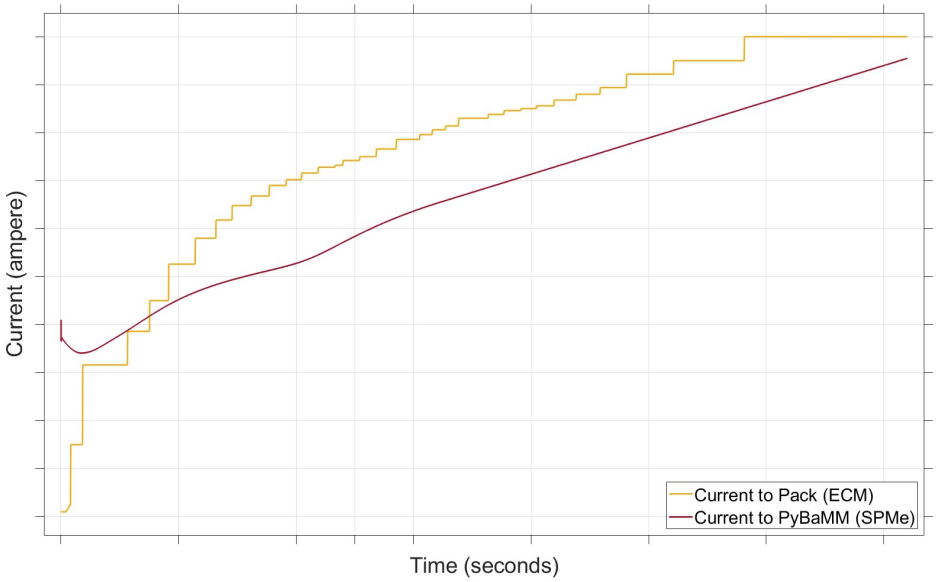

Figure 4.20: Current profile of the Volvo automotive cell

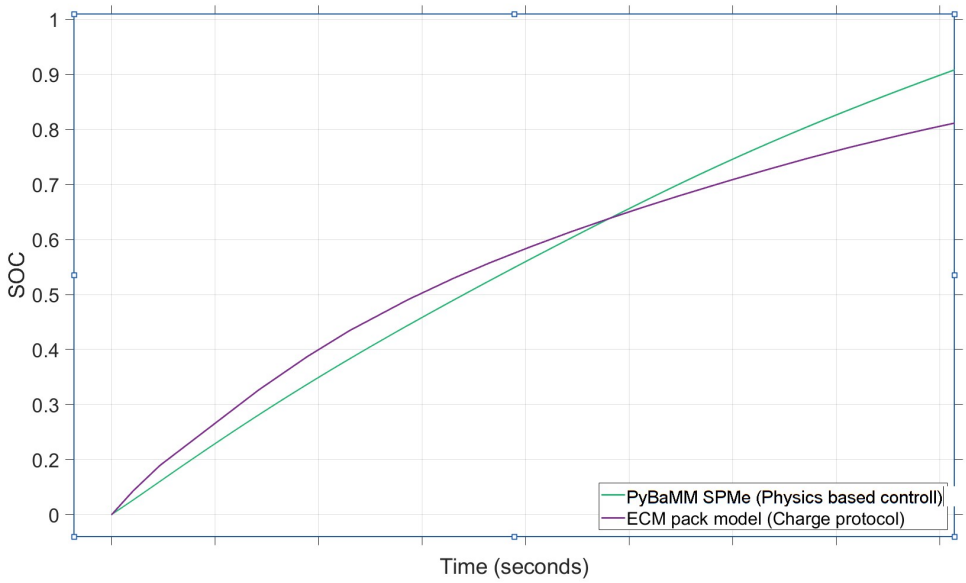

Figure 4.21: SOC for the Volvo automotive cell

Using the current controller based on the anode potential the model uses a higher charging current through the majority of the charge. This means that when the charging scheme is controlled through the anode potential, the battery reaches 80% SOC 18% faster. This can be seen in figure 4.21.

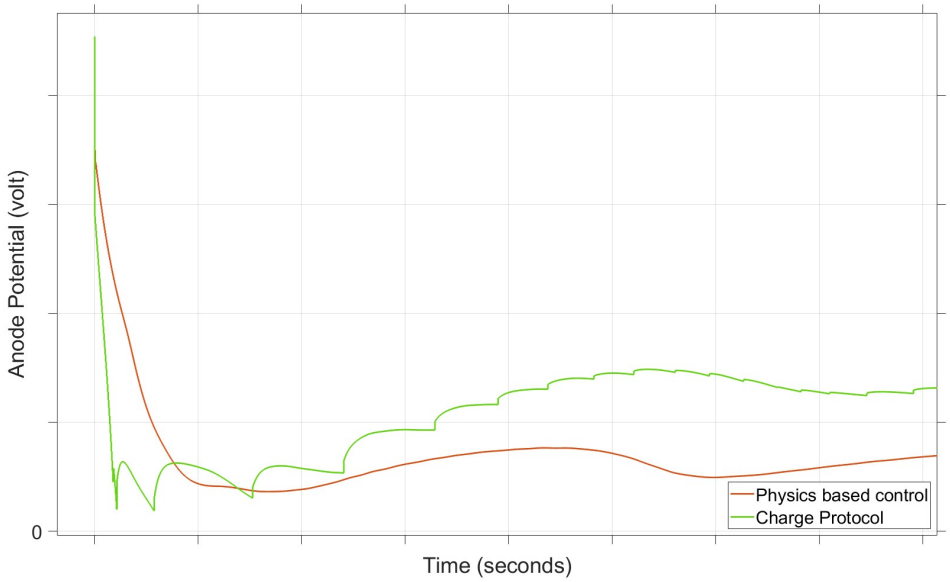

Figure 4.22: Anode Potential for the Volvo automotive cell

Figure 4.22 shows the anode potential during fast charge for the two different control methods, showing that the physics-based control keeps the anode potential closer to 0 during the cycle. It can be seen that the charge protocol leads to an anode potential close to 0 very early in the charge, as a result of its high initial current. The anode potential for the charge protocol then rises again as the current is lowered throughout the charge. As the physics-based control is monitoring the potential in real time, it can input a higher current but still keep the anode potential above 0. The model can be tuned to achieve the desired safety margin.

As the charge protocol is designed to be used for both fresh and aged cells, the current is set lower to allow for margin to avoid lithium plating. Having a physics-based controller that can adjust the charging current based on real-time cell parameters can instead lead to the current controller always using the max current rate available based on the SOH of the cells in a pack.

4.3.5 Cycling

In these simulations all modules in the Simscape pack used ECM and the physics-based modeling was exclusively done in PyBaMM. This was done to cut down on computational load as the SPMe based modeling is computationally heavier compared to the SPMe modeling in PyBaMM.

In figure 4.23 the SOC for the PyBaMM cell, ECM, and SPMe modules in the pack can be seen. The simulation represents five cycles of fast charging from 10% SOC to 80% SOC and then discharging during driving down to 10% SOC again followed by one final charge. The total sequence took 55 000 seconds or approximately 15 hours and 16 minutes. As in the fast charging simulations the ECM modules pull ahead

during the fast charge due to them ignoring internal electrochemical dynamics.

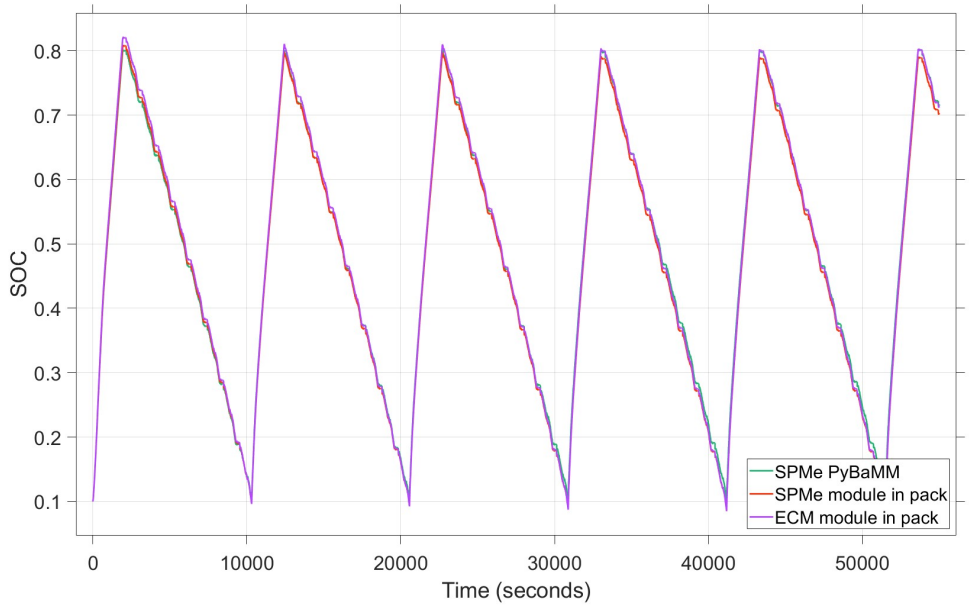

Figure 4.23: SOC during cycling from 10% SOC to 80% SOC

The pack current can be seen in figure 4.25. During driving there is more oscillations in the current due to it being taken from a real test drive. The pack voltage can be seen in figure 4.24 and similarly to the pack current it oscillates during driving, this as a result of the charging current.

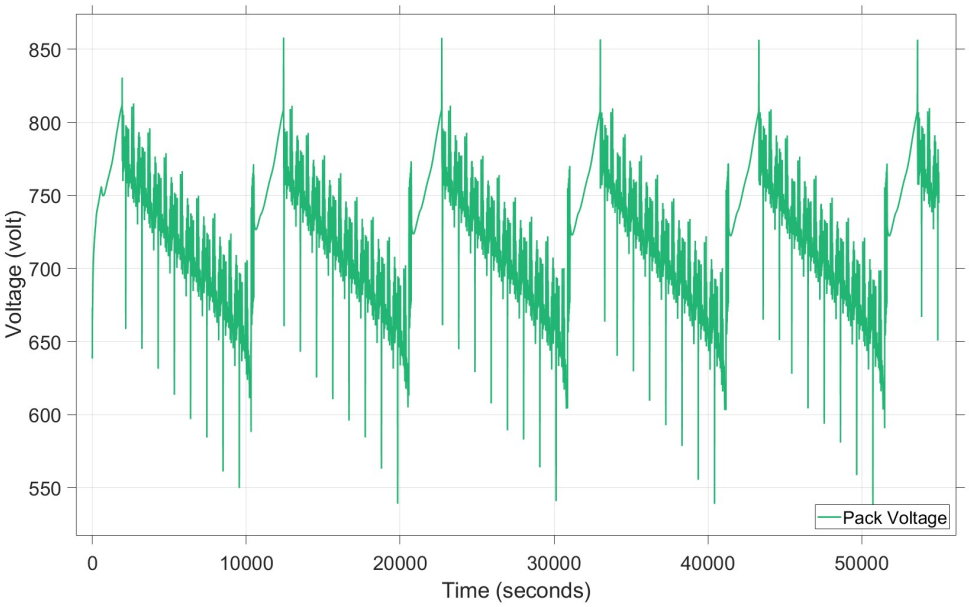

Figure 4.24: Pack voltage profile during cycling from 10% SOC to 80% SOC

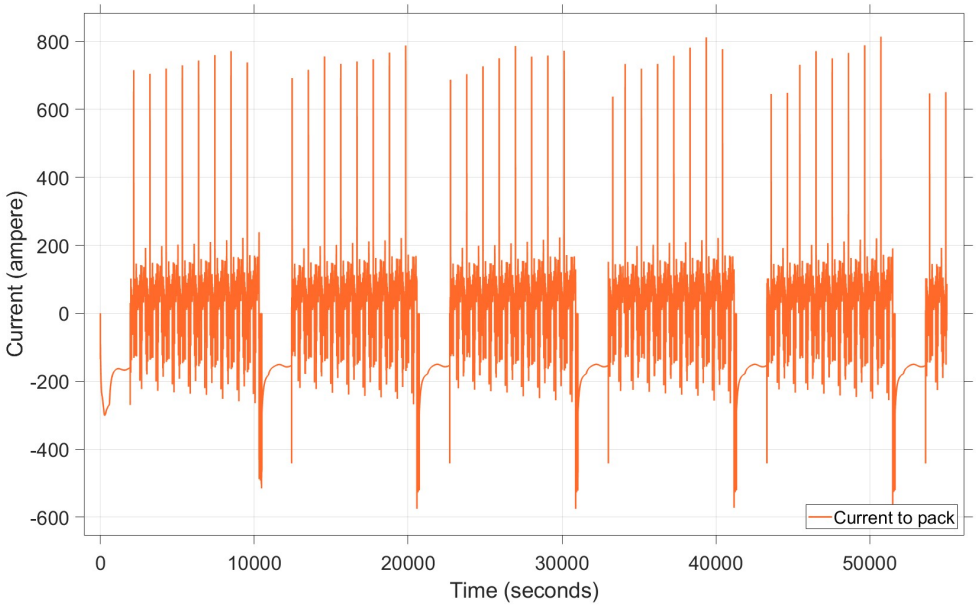

Figure 4.25: Pack current profile during cycling from 10% SOC to 80% SOC

In figure 4.26 the temperature of the pack during the cycles can be seen. The temperature of the pack during fast charge is kept at the same level as the fast charging simulations done earlier in the project. During discharge, the temperature remains constant at around 308 K. It can also be seen that the temperature is kept steady between cycles and does not increase notably over time. This shows that the thermal management system is able to handle cycling over time.

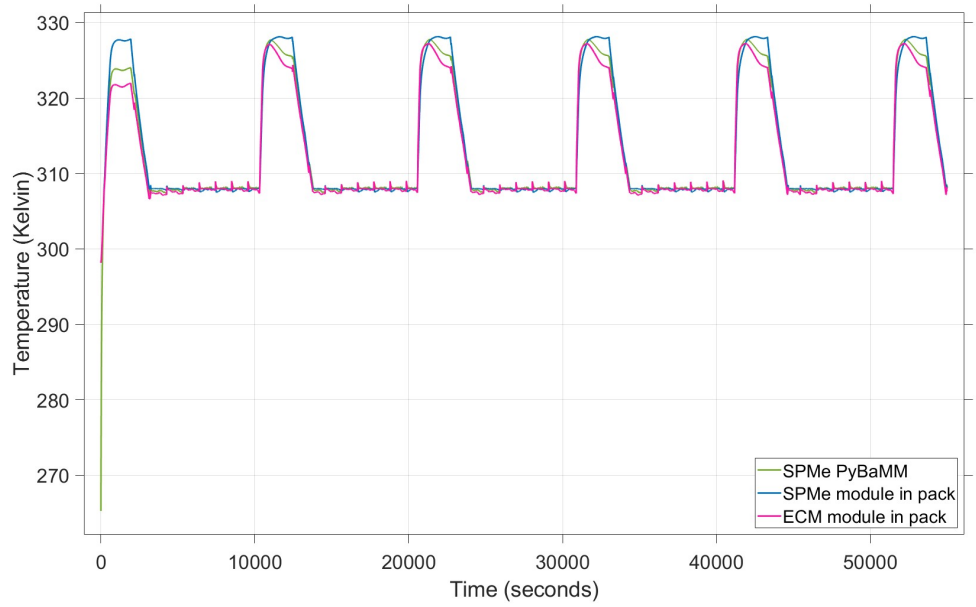

Figure 4.26: Pack temperature during cycling from 10% SOC to 80% SOC

The anode potential during the cycling can be seen in figure 4.27. When the switch

between discharge and charge is made, the anode potential reaches its lowest. This is due to the sudden increase in current from discharging to a high charge rate. Consequently, this is the time that the battery is at the highest risk of lithium plating.

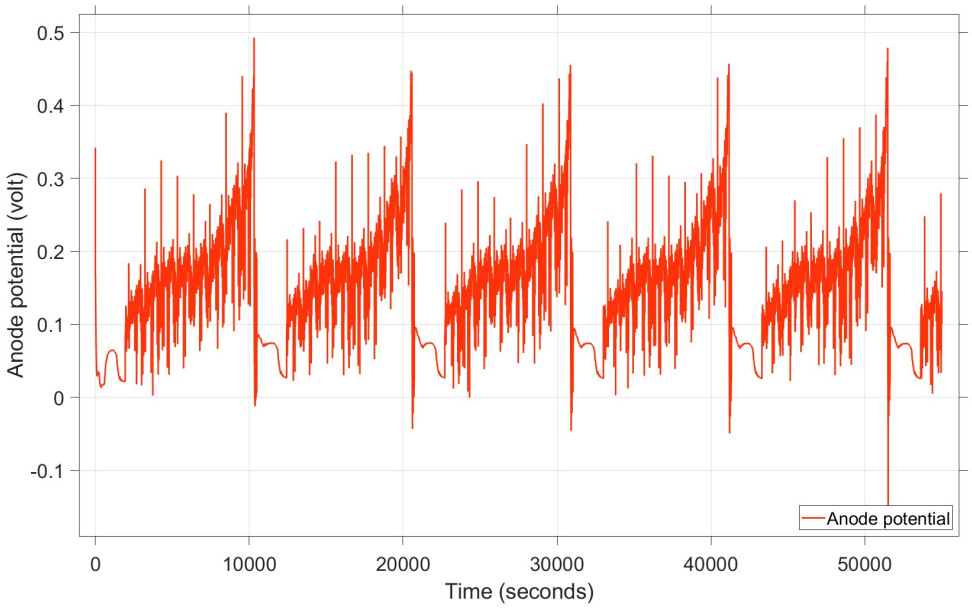

Figure 4.27: Anode potential during cycling from 10% SOC to 80% SOC

In figure 4.28 the lithium plating that occurs during the charging of the battery is shown, however in this case the lithium plating settings in PyBaMM are set to partially reversible. During this simulation there are only a few cycles and all the lithium plating that occurs is reversible, this can be seen as it goes down to zero again between cycles. If an even longer simulation were run, it would most probably be seen that some of the lithium plating remained between cycles.

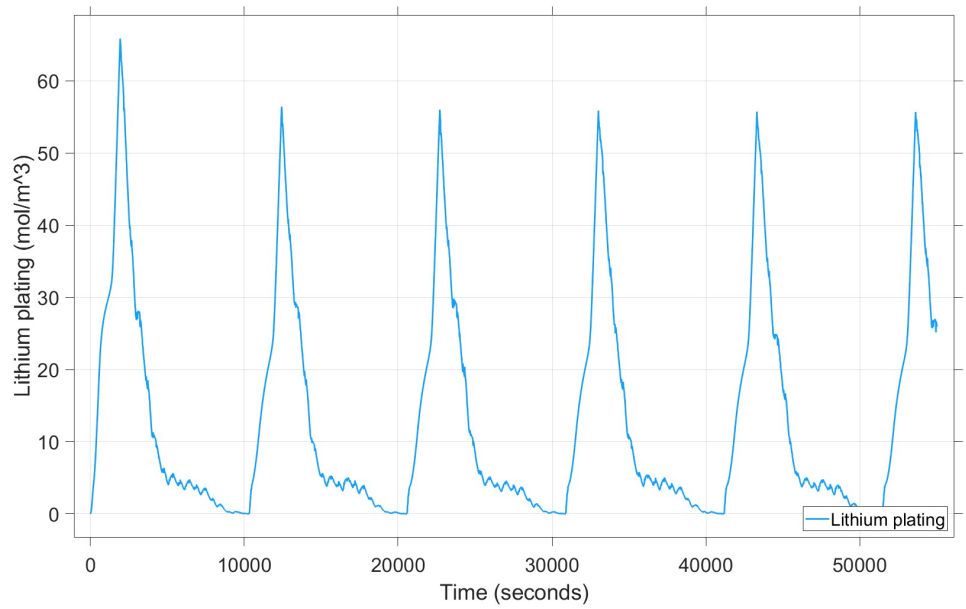

Figure 4.28: Lithium plating measured by PyBaMM during cycling from 10% SOC to 80% SOC

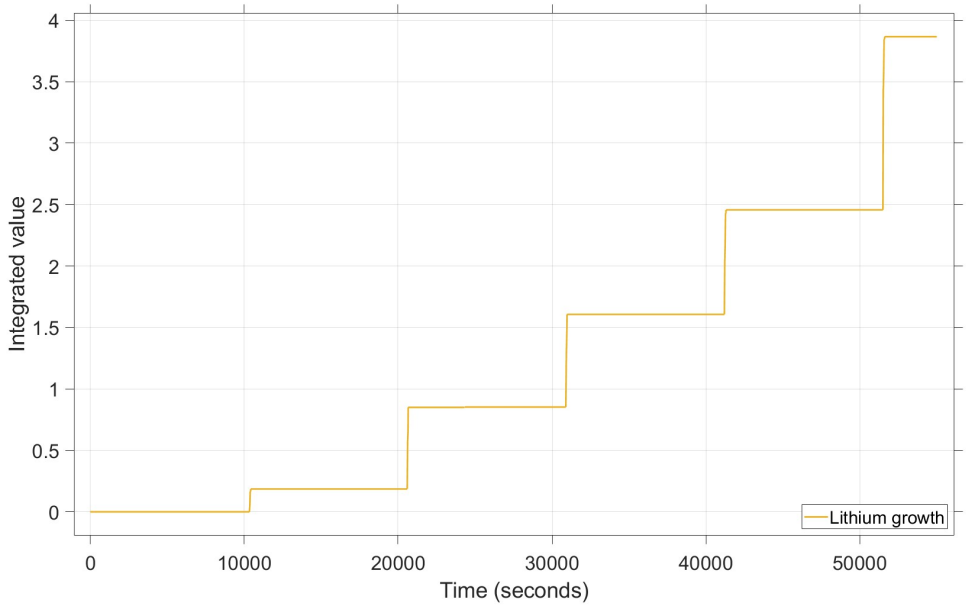

Figure 4.29: Result from integration of the negative electrode voltage when it was under 0 during cycling from 10% SOC to 80% SOC

To be able to quantify the amount of lithium plating and how it changed over time and could add up over time, an integrator was used to be able to evaluate this. The results of the integrator can be seen in figure 4.29. Here, it can be clearly seen that the anode potential takes on values below zero for longer periods of time as the cycle goes on. This shows that the model can identify aging factors over time when

the battery is cycled. The longer the sequence, the greater the risk of lithium plating.

This use case shows that the implementation of the PyBaMM monitor in the model offers new uses of the model that would not have been possible in Simulink and Simscape alone. The computational load can be decreased by using PyBaMM for the physics-based modeling cutting down the simulation time for these kinds of longer simulations and the PyBaMM monitor also allows the model to simulate the aging effects occurring in the battery pack.

5
Discussion

5.1 Sustainability

This project has focused on developing methods using physics-based models for software control of battery packs in electric vehicles. Using physics-based models for software control has the possibility to increase the lifetime of batteries and decrease the carbon footprint of electric vehicles. Both emissions from production and the climate impact of the mining materials for batteries would decrease if it were possible to get more use from batteries.

Since the electric vehicle market is growing, the need for materials such as lithium will only get larger. There are many ways to get as much use as possible out of the materials. Recycling and refurbishment are important for when batteries are no longer sufficient for use in electric vehicles, but being able to minimize the aging of them will prolong the period in which they can be used for their intended purpose. This can in turn reduce the environmental strain from the production of electric vehicles.

Longer lasting and more efficient batteries can reduce ownership costs, making electric vehicles more attractive to consumers. This can accelerate the rate of customers that transition from fossil fuel-driven vehicles to electric vehicles and in turn lower the emissions caused by cars and other vehicles.

5.2 Ethics

There are ethical concerns about the mining of materials for electric vehicles such as lithium, nickel, and cobalt. The mining of these materials is often done in developing nations with very poor worker conditions. So, developing methods for software control that have the ability to minimize the aging of battery cells and prolong their lifespan can, in the long term, reduce the need for these materials that come from these mining facilities. This is far from a solution to the problem, but can definitely be a step in the right direction.

5.3 Future Work

This report shows a method for how to implement different physical-based properties in the software control for battery packs intended for use in electric vehicles. More evaluation of the accuracy of the model can be done to make sure that the model works as closely as possible to a real battery. To develop the current control to be more optimal as a possibility to increase the efficiency of the fast charge case. With more parametrization of cells at Volvo cars it could be possible to run simulations based on test drives and evaluate the results as was done in the validation model in this project. This was not possible to do in this project, since the parametrization of the Volvo cars cells was lacking in both thermal behavior and aging dynamics to run physics-based simulations on them to the extent that was needed to implement in the full model. This is definitely an area that could be delved deeper into in the future.

Further investigation in the aging parameters and longer simulations with more cycles is needed to get a clearer view of how aging impacts the battery pack after long-term use. In this thesis, the aging parameters were implemented manually, but since the PyBaMM model has the possibility to simulate aging over time, that is something to look at in the future. In the case where the effects of aging were analyzed for a specific use, the simulations were not long enough to get a detailed understanding of the effects of aging.

Another possibility for further development could be to introduce deviation between the cells to get a more realistic EV battery pack and to see how the model handles this. Introducing deviations into the cells that are based on error margins from suppliers would be a very interesting next step for the project. This can be done in both Simscape or by introducing more PyBaMM modules into the model. To do it in Simscape requires more computational power and would slow down the simulations.

What could be interesting is to add some faults to the battery to see how the models handle that kind of situation, for example, some short circuit fault or introduce a thermal runaway scenario.

The fast charging case with the production cell requires more parametrization of the battery to obtain a more accurate result, as there is a lack of thermal and aging parameters in the existing parameter set. Tests with a aged production cells would give a better understanding of how using a psychical based control compared to a charge protocol can be advantageous.

6
Conclusion

For this thesis, a model was developed to model a battery pack used in an electric vehicle. The goal was to create a model that had the abilities of a physics-based model but with a lower computational load. This was achieved by creating a hybrid model with physic-based SPMe models and empirical based ECM models. The model was built in Simulink and Simscape battery with the addition of PyBaMM cells that acted as monitors.

Using a hybrid model for battery pack modeling was found to be a working method to be able to use internal electrochemical dynamics for control and analysis at lower computational load compared to a fully physics-based model. By implementing PyBaMM in the Simscape model, gave the ability to model aging and see how different usage of the battery affect aging. When comparing the use of Simscape and PyBaMM to model physical-based aspects, the PyBaMM model is a better option as it has considerably lower computational load and gives the options to add aging characteristics, and thereby giving the simulations a more realistic output. This model is also adaptable as the battery used can be changed as long as the right parametrization is available.

When using the model to simulate fast charging, the model was able to take into account parameters related to aging and give us the ability to control the charging current to mitigate aging of the battery pack. This is something that would not have been possible with a fully ECM based model.

Fast charging simulation were also ran where SEI growth was added manually to simulate aged cells with reduced capacity. The results of the current and voltage differences between the different simulations show that the model can simulate aged batteries and adapt the input current to keep the battery operating safely without increasing the risk of further aging by keeping the anode potential above zero. Similarly, fast charging simulations at different initial temperatures were also ran. In these simulations, clear differences were seen showing that the model can differentiate between the different cases. The physics-based current controller was able to adapt to all cases and perform a fast charge without the anode potential going below zero and increasing the risk of aging.

The SPMe PyBaMM module with the aging parameters had a lower voltage compared to the other modules, approximately 0.065 V at the same SOC during the entire charging cycle. The ideal PyBaMM SPMe can also be seen to follow the

SPMe Simscape model well, which means that the battery pack can consist of only ECM and instead add more PyBaMM monitors as they do not impact the computational load as much as the SPMe model in Simscape does, adding one module per string increased the simulation time by approximately 25% while adding another PyBaMM cell to the models adds approximately 4% to the simulation time.

Looking at the Volvo automotive battery, it was able to go from 10% to 80% SOC, 18% faster when using physics-based control compared to the charge protocol. The charge was also faster without an increased risk of aging, showing the advantages and possibilities of using the physical-based control. Using a physics-based controller for fast charging would enable the controller to utilize the maximum available current rate based on the real-time cell parameters of the battery.

The aging simulation of the model gave promising results, as it could monitor the lithium plating in the battery during cycling, showing that the developed method can take aging parameters into account. The integrator applied to the anode potential was able to indicate when there was a risk of non-reversible lithium plating. However, to obtain a result of the direct impact of non-reversible lithium plating, longer simulations with more cycles are needed.

References

[1] International Energy Agency. "Global EV Outlook 2024: Trends in Electric Cars." Accessed: 2024-04-27. (2024), [Online]. Available: https://www.iea.org/reports/global-ev-outlook-2024/trends-in-electric-cars.

[2] X. Lin, Y. Kim, S. Mohan, J. B. Siegel, and A. G. Stefanopoulou, "Modeling and estimation for advanced battery management," *Annual Review of Control, Robotics, and Autonomous Systems*, vol. 2, no. Volume 2, 2019, pp. 393–426, 2019, ISSN: 2573-5144. DOI: https://doi.org/10.1146/annurev-control-053018-023643. [Online]. Available: https://www.annualreviews.org/content/journals/10.1146/annurev-control-053018-023643.

[3] B. Yann Liaw, G. Nagasubramanian, R. G. Jungst, and D. H. Doughty, "Modeling of lithium ion cells—a simple equivalent-circuit model approach," *Solid State Ionics*, vol. 175, no. 1, pp. 835–839, 2004, Fourteenth International Conference on Solid State Ionics, ISSN: 0167-2738. DOI: https://doi.org/10.1016/j.ssi.2004.09.049. [Online]. Available: https://www.sciencedirect.com/science/article/pii/S0167273804006678.

[4] A. Basia, Z. Simeu-Abazi, E. Gascard, and P. Zwolinski, "Review on state of health estimation methodologies for lithium-ion batteries in the context of circular economy," *CIRP Journal of Manufacturing Science and Technology*, vol. 32, pp. 517–528, 2021, ISSN: 1755-5817. DOI: https://doi.org/10.1016/j.cirpj.2021.02.004. [Online]. Available: https://www.sciencedirect.com/science/article/pii/S1755581721000249.

[5] G. Liu, L. Lu, H. Fu, *et al.*, "A comparative study of equivalent circuit models and enhanced equivalent circuit models of lithium-ion batteries with different model structures," *2014 IEEE Conference and Expo Transportation Electrification Asia-Pacific (ITEC Asia-Pacific)*, pp. 1–6, 2014. [Online]. Available: https://api.semanticscholar.org/CorpusID:11825103.

[6] M. Doyle, T. F. Fuller, and J. Newman, "Modeling of galvanostatic charge and discharge of the lithium/polymer/insertion cell," *Journal of The Electrochemical Society*, vol. 140, no. 6, p. 1526, Jun. 1993. DOI: 10.1149/1.2221597. [Online]. Available: https://dx.doi.org/10.1149/1.2221597.

[7] A. Jokar, B. Rajabloo, M. Désilets, and M. Lacroix, "Review of simplified pseudo-two-dimensional models of lithium-ion batteries," *Journal of Power Sources*, vol. 327, pp. 44–55, 2016, ISSN: 0378-7753. DOI: https://doi.org/10.1016/j.jpowsour.2016.07.036. [Online]. Available: https://www.sciencedirect.com/science/article/pii/S0378775316308916.

[8] N. T. Tran, M. Vilathgamuwa, T. Farrell, and S. S. Choi, "Matlab simulation of lithium ion cell using electrochemical single particle model," in *2016 IEEE*

2nd Annual Southern Power Electronics Conference (SPEC), Auckland, New Zealand, 2016, pp. 1–6. DOI: 10.1109/SPEC.2016.7846195.

[9] L. Raviteja and G. Gurrala, "A review of lithium-ion battery physics-based models," in *2023 IEEE Power & Energy Society General Meeting (PESGM)*, IEEE, 2023, pp. 1–5. DOI: 10.1109/PESGM52003.2023.10252738.

[10] S. G. Marquis, V. Sulzer, R. Timms, C. P. Please, and S. J. Chapman, "An asymptotic derivation of a single particle model with electrolyte," *Journal of The Electrochemical Society*, vol. 166, no. 15, A3693, Nov. 2019. DOI: 10.1149/2.0341915jes. [Online]. Available: https://dx.doi.org/10.1149/2.0341915jes.

[11] P. Developers, *Single particle model with electrolyte (spme)*, Accessed: 2025-01-13, 2025. [Online]. Available: https://docs.pybamm.org/en/stable/source/examples/notebooks/models/SPMe.html.

[12] S. E. J. O'Kane, W. Ai, G. Madabattula, *et al.*, "Lithium-ion battery degradation: How to model it," *Physical Chemistry Chemical Physics*, vol. 24, no. 13, pp. 7909–7922, 2022, ISSN: 1463-9084. DOI: 10.1039/d2cp00417h. [Online]. Available: http://dx.doi.org/10.1039/D2CP00417H.

[13] C.-H. Chen, F. B. Planella, K. O'Regan, D. Gastol, W. D. Widanage, and E. Kendrick, "Development of experimental techniques for parameterization of multi-scale lithium-ion battery models," *Journal of The Electrochemical Society*, vol. 167, no. 8, p. 080 534, May 2020. DOI: 10.1149/1945-7111/ab9050. [Online]. Available: https://dx.doi.org/10.1149/1945-7111/ab9050.

[14] P. Team, *Ptbamm*, https://pybamm.org/, [Online; accessed 24-Oct-2024], 2024.

[15] L. Liu and M. Zhu, "Modeling of sei layer growth and electrochemical impedance spectroscopy response using a thermal-electrochemical model of li-ion batteries," *ECS Transactions*, vol. 61, no. 27, p. 43, Oct. 2014. DOI: 10.1149/06127.0043ecst. [Online]. Available: https://dx.doi.org/10.1149/06127.0043ecst.

[16] M. Petzl and M. A. Danzer, "Nondestructive detection, characterization, and quantification of lithium plating in commercial lithium-ion batteries," *Journal of Power Sources*, vol. 254, pp. 80–87, 2014, ISSN: 0378-7753. DOI: https://doi.org/10.1016/j.jpowsour.2013.12.060. [Online]. Available: https://www.sciencedirect.com/science/article/pii/S0378775313020387.

[17] F. S. Hwang, T. Confrey, C. Reidy, *et al.*, "Review of battery thermal management systems in electric vehicles," *Renewable and Sustainable Energy Reviews*, vol. 192, p. 114 171, 2024, ISSN: 1364-0321. DOI: https://doi.org/10.1016/j.rser.2023.114171. [Online]. Available: https://www.sciencedirect.com/science/article/pii/S1364032123010298.

[18] X.-G. Yang, S. Ge, T. Liu, Y. Leng, and C.-Y. Wang, "A look into the voltage plateau signal for detection and quantification of lithium plating in lithium-ion cells," *Journal of Power Sources*, vol. 395, pp. 251–261, 2018, ISSN: 0378-7753. DOI: https://doi.org/10.1016/j.jpowsour.2018.05.073. [Online]. Available: https://www.sciencedirect.com/science/article/pii/S0378775318305573.

[19] J. S. Edge, S. O'Kane, R. Prosser, *et al.*, "Lithium ion battery degradation: What you need to know," *Phys. Chem. Chem. Phys.*, vol. 23, pp. 8200–8221, 14 2021. DOI: 10.1039/D1CP00359C. [Online]. Available: http://dx.doi.org/10.1039/D1CP00359C.

[20] X. Zhao, Y. Yin, Y. Hu, and S.-Y. Choe, "Electrochemical-thermal modeling of lithium plating/stripping of $li(ni_{0.6}mn_{0.2}co_{0.2})o_2$/carbon lithium-ion batteries at subzero ambient temperatures," *Journal of Power Sources*, vol. 418, pp. 61–73, 2019, ISSN: 0378-7753. DOI: 10.1016/j.jpowsour.2019.02.001.

[21] X. Duan and G. Naterer, "Heat transfer in phase change materials for thermal management of electric vehicle battery modules," *International Journal of Heat and Mass Transfer*, vol. 53, no. 23, pp. 5176–5182, 2010, ISSN: 0017-9310. DOI: https://doi.org/10.1016/j.ijheatmasstransfer.2010.07.044. [Online]. Available: https://www.sciencedirect.com/science/article/pii/S0017931010004229.

[22] M. Shahjalal, T. Shams, M. E. Islam, *et al.*, "A review of thermal management for li-ion batteries: Prospects, challenges, and issues," *Journal of Energy Storage*, vol. 39, p. 102 518, 2021, ISSN: 2352-152X. DOI: https://doi.org/10.1016/j.est.2021.102518. [Online]. Available: https://www.sciencedirect.com/science/article/pii/S2352152X21002668.

[23] X. Li, J. Zhao, J. Duan, *et al.*, "Simulation of cooling plate effect on a battery module with different channel arrangement," *Journal of Energy Storage*, vol. 49, p. 104 113, 2022, ISSN: 2352-152X. DOI: https://doi.org/10.1016/j.est.2022.104113. [Online]. Available: https://www.sciencedirect.com/science/article/pii/S2352152X22001499.

[24] MathWorks, *U-shaped channels*, Accessed: 2025-01-13, 2025. [Online]. Available: https://se.mathworks.com/help/simscape-battery/ref/ushapedchannels.html.

[25] P. Developers, *Thermal models*, Accessed: 2025-01-13, 2025. [Online]. Available: https://docs.pybamm.org/en/stable/source/examples/notebooks/models/thermal-models.html.

[26] Y.-S. Kim and S. W. Roh, *Lg inr21700 m50 product specification*, Version: Tentative, Document No.: LRB-PS-CY18.2Wh-M50, LG Chem, Aug. 2016. [Online]. Available: https://www.dnkpower.com/wp-content/uploads/2019/02/LG-INR21700-M50-Datasheet.pdf.

[27] S. E. J. O'Kane, W. Ai, G. Madabattula, *et al.*, "Lithium-ion battery degradation: How to model it," *Phys. Chem. Chem. Phys.*, vol. 24, pp. 7909–7922, 13 2022. DOI: 10.1039/D2CP00417H. [Online]. Available: http://dx.doi.org/10.1039/D2CP00417H.

DEPARTMENT OF ELECTRICAL ENGINEERING
CHALMERS UNIVERSITY OF TECHNOLOGY
Gothenburg, Sweden
www.chalmers.se

CHALMERS
UNIVERSITY OF TECHNOLOGY